Supplementary Information

Buoyant magnetic milliswimmers reveal design rules for optimizing microswimmer performance

Emma Benjaminson,[a‡] Taryn Imamura,[a‡] Aria Lorenz,[a] Sarah Bergbreiter,[abc]
Matthew Travers,[c] and Rebecca E. Taylor[*abd]

[a]Department of Mechanical Engineering, Carnegie Mellon University, 5000 Forbes Avenue, Pittsburgh, USA. E-mail: bex@andrew.cmu.edu; Fax: +1-412-268-3348; Tel: +1-412-268-2500

[b]Electrical and Computer Engineering, Carnegie Mellon University, 5000 Forbes Avenue, Pittsburgh, USA.

[c]The Robotics Institute, Carnegie Mellon University, 5000 Forbes Avenue, Pittsburgh, USA.

[d]Department of Biomedical Engineering, Carnegie Mellon University, 5000 Forbes Avenue, Pittsburgh, USA.

Contents

1   Model Parameters

In this section, we present the parameters we used and derived for our models of the cylindrical and spherical swimmers. First we present the calculations, and then the final values for each system are presented in tables at the end of this section.

1.1   Torsion Spring Constant

In our experimental realization of our milliswimmer, the torsion spring that connects the two links is a small beam with a circular cross section. We can compute the bending stiffness of the beam and use it as our value for κ. First we model the beam as a fixed cantilever (i.e. fixed to one of the links) with a moment load applied at the free end:

$$\delta_{max} = \frac{ML^2}{2EI}$$

$$M = \frac{2EI}{L}\frac{\delta_{max}}{L}$$

Where δ_{max} is the maximum deflection of the end of the beam, M is the bending moment, L is the length of the beam, E is the beam's Young's modulus and I is the beam's area moment of inertia. We rearrange the equation to take the same form as the expression for a torsion spring's torque, $\tau = \kappa\theta$, where $\tau = M$, $\theta = \frac{\delta_{max}}{L}$ and $\kappa = \frac{2EI}{L}$. So finally we can solve for κ as:

$$\kappa = \frac{2EI}{L} = \frac{2E(\frac{\pi}{4}r^4)}{L}$$
$$= \frac{2(5.1\times10^9N/m^2)\left(\frac{\pi}{4}(5\times10^{-6})^4\right)}{(39.5\times10^{-6})}$$
$$= 1.2676\times10^{-7}Nm/rad$$

For our weaker torsion spring, we increased the length of the joint from 39.5×10^{-6}m to 79×10^{-6}m to obtain:

$$\kappa = \frac{2(5.1\times10^9)(\frac{\pi}{4}(5\times10^{-6})^4)}{(79\times10^{-6})}$$
$$= 6.3379\times10^{-8}Nm/rad$$

We obtained the Young's modulus of cured IP-S (the photoresin used to make the milliswimmers) from the manufacturer [1].

1.2   Hydrodynamic Drag Coefficient

There is an analytical definition for the hydrodynamic drag coefficient provided in the literature per [2, 3, 4] (more details below) but we found that this analytical expression tended to underestimate the drag coefficient for our milliswimmer systems. We found that when we generated model predictions using our second order system, the model significantly overestimated the net velocities of the swimmers. We hypothesize that, since our swimmers are at the milliscale and have Reynolds numbers that range from approximately 0.1 to 1 (depending on the actuation frequency), the assumption that we can describe the drag using a low Reynolds number definition may not be accurate.

Furthermore, we note that the outer surface of our milliswimmers is not perfectly smooth - our SEM images indicate that the TPP process imparts nanoscale print lines that interrupt the surface finish. Other necessary design features also interrupt the outer profile, including the drainage ports on the top surface, the flat surface necessary to adhere the swimmer to the glass coverslip, and the nail polish added for visibility. Since the milliswimmer is moving through Percoll, which is a fluid comprised of silica beads (coated in PVP) of diameters approximately 30nm suspended in water, the silica beads are on the same length scale as these surface imperfections. This could lead to additional interactions between the fluid and the milliswimmer's outer surface that further reduce its velocity beyond what we estimate with an analytical expression developed for low Reynolds number situations with idealized shapes.

Therefore, we used gradient descent to find values of k_t that closely matched our experimental data, and compared them to the analytical estimates. Specifically, we used a starting value of k_t, and generated a model prediction for

Seed	Nominal	Large Aspect Ratio	Weak κ
1.7	1.8323 (5.3528×10^{-4})*	1.7248 (1.0136×10^{-4})	1.6105 (8.2273×10^{-4})*
0.8	0.8261 (2.3894×10^{-4})	1.2021 (1.2075×10^{-4})	0.2974 (5.5855×10^{-5})
0.5	0.4092 (7.9948×10^{-5})**	1.2045 (1.1987×10^{-4})	0.2776 (4.1880×10^{-5})**
Average	**0.6176**	**1.3771**	**0.2875**

Table S1: Round 1 gradient descent results for nominal, large aspect ratio and weak torsion spring designs - value of k_t is reported with MAE error in parentheses (units of k_t are $\frac{Ns}{m}$ and units of MAE error are m/s). *Excluded as outlier from calculation of average. **This was the last value with decreasing MAE before the algorithm diverged.

the net velocities over the experimentally observed frequency range $[1, 10]$Hz. We calculated the objective function as the mean absolute error (MAE) between the model prediction and the mean of the experimentally observed data (averaged over the 10 frequencies we tested experimentally). We then used the central differencing scheme to compute the gradient of the objective function around this value of k_t and used a gradient descent update function to adjust the value of k_t:

$$k_{t,new} = k_{t,old} - \eta \nabla f(k_t)$$

Where η is the learning rate and $f(k_t)$ is the objective function (i.e. the MAE between the model and the experimental data).

We ran the gradient descent algorithm in two rounds. First we applied gradient descent to 4 cylindrical designs (nominal, large aspect ratio, weak torsion spring and safety factor of 1.1) at a range of initial values for k_t within the search space $k_{t,initial} = \{1.7, 0.8, 0.5\}$ to find approximate values of k_t in each case. We ran the gradient descent algorithm for this first round with $\eta = 100$ and up to a maximum of 10 iterations or until the MAE was less than 3×10^{-5}m/s, whichever came first. We then calculated the average k_t value from each of the k_t values found at the end of 10 iterations given each of the 3 seeds in the first round. Note that if one of the final k_t values was a significant outlier (by comparing its MAE with the other k_t values), then we excluded it from the calculation of the average.

We then used these averaged values of k_t for each swimmer shape from the first round as a "hot start" for a second round of gradient descent to further refine the estimate and reduce the MAE error. In the second round we kept $\eta = 100$ and ran up to a maximum of 10 iterations. The purpose here was to continue searching in the region of the search space that was most likely to contain a value of k_t that minimized the MAE given what we had learned from Round 1. We selected the final value of k_t as the value that minimized the error over the 10 iterations, or the value that achieved MAE error of less than 1×10^{-5}m/s, whichever came first. Note that occasionally the gradient descent algorithm diverged and so we chose the k_t value with the minimum MAE before the divergence occurred as our final value.

The results of the first round of gradient descent for the nominal, large aspect ratio and weak torsion spring swimmers are shown in Table S1, and the second round, compared with the analytical k_t values, in Table S4. The same results for first and second rounds for the swimmer with safety factor 1.1 in both Percoll and the Percoll/water mixture, as well as for test conditions with $\beta =2$ and 3, are reported in Tables S2 and S4. The calculations for the analytical k_t values are shown below.

Note that we also performed gradient descent to fit k_t to the same nominal swimmer when actuated with magnetic fields with $\beta > 1$. Although the same k_t value should be applicable for all cases, we wanted to see if we could better fit the model to the data for these particular actuation schemes. We found that the k_t values we were able to fit to the data at higher β were similar to the k_t value for the nominal cylindrical swimmer when $\beta = 1$. We tried using $k_t = 0.3247$ (the nominal value) to fit to the $\beta > 1$ experimental data and found the error was comparable to that achieved by specially fitting k_t for this particular case. We found the error for $\beta = 2$ was 5.7851×10^{-4} and for $\beta = 3$ the error was 3.9350×10^{-4}m/s. These values were obtained for B_x^+. We also noted that during the second round of gradient descent, we had to adjust the learning rate from 100 to 10 to avoid taking steps that were too large. This suggests that the behavior of the model changes more steeply when β is larger. The higher β values lead to larger sweep angles, which means that the swimmers are moving more quickly to sweep through that angle every cycle. The higher velocities may push the swimmer further into a higher Reynolds number configuration, making the assumptions in our dynamics model less applicable.

Seed	SF 1.1 (Percoll)	SF 1.1 (Percoll/water)	Nominal $\beta = 2$	Nominal $\beta = 3$
1.7	2.064 (5.8642×10^{-4})*	1.3282 (3.4022×10^{-4})*	1.7809 (6.3136×10^{-4})*	1.4416 (8.2408×10^{-4})*
0.8	0.7845 (1.5201×10^{-4})	0.6661 (1.3182×10^{-4})*	0.4032 (2.7385×10^{-4})**	0.4403 (3.8878×10^{-4})**
0.5	0.3901 (2.3539×10^{-4})	0.3525 (2.8058×10^{-5})	2.3370 (5.9539×10^{-4})*	2.4287 (7.1558×10^{-4})*
Average	**0.5873**	**0.3525**	**0.4032**	**0.4403**

Table S2: Round 1 gradient descent results for swimmer with safety factor of 1.1 in Percoll and Percoll/water mixture. Value of k_t is reported with MAE error in parentheses (units of k_t are $\frac{Ns}{m}$ and units of MAE error are m/s). *Excluded as outlier from calculation of average.

Value	Nominal	Large Aspect Ratio	Weak κ
Initial Seed	0.6176	1.3771	0.2875
Final Value (GD)	**0.3247****	**1.6489**	**0.2875****
Error (MAE)	4.7721×10^{-5}	9.6929×10^{-5}	4.9270×10^{-5}
Analytical Value	**0.0680**	**0.0453**	**0.0680**

Table S3: Round 2 gradient descent results for all swimmers. Units of k_t are $\frac{Ns}{m}$ and units of MAE error are m/s. *Excluded as outlier from calculation of average. **This was the last value with decreasing MAE before the algorithm diverged.

When we compared the final values found using gradient descent against the values we calculated using the literature definition as presented below, we found that there were two key differences. The first was that our values found using gradient descent were 1-2 orders of magnitude larger - we discussed our hypotheses as to why this is true above. Secondly, the analytical expression for k_t predicts that swimmers with larger aspect ratios will see smaller drag coefficients - this same pattern persists for drag coefficients at higher Reynolds number as well, where cylinders with longer lengths tend to have smaller drag coefficients. However, we found that the values computed with gradient descent show a larger value of k_t for the swimmer with the larger aspect ratio, reversing this trend. This could be a further indication that the surface roughness is interacting with the microbeads in the Percoll, and therefore links with larger surface area are seeing more drag than links with less surface area.

Here we present the calculated values of k_t for our cylindrical swimmer designs. We can define k_t as the drag coefficient for a cylinder per [2, 3, 4]:

$$k_t = \frac{2\pi\eta}{\ln(L/a)}$$

Where η is the dynamic viscosity of the fluid, L is the length and a is the radius of the cylinder. We use the known

Value	SF 1.1 (Percoll)	SF 1.1 (Percoll/water)	Nominal $\beta = 2$	Nominal $\beta = 3$
Initial Seed	0.5873	0.3525	0.4032	0.4403
Final Value (GD)	**0.4002****	**0.3525****	**0.3546****	**0.4354**
Error (MAE)	3.1920×10^{-5}	2.8058×10^{-5}	1.3797×10^{-4}	3.8865×10^{-4}
Analytical Value	**0.0680**	**0.0680**	**0.0680**	**0.0680**

Table S4: Round 2 gradient descent results for all swimmers. Units of k_t are $\frac{Ns}{m}$ and units of MAE error are m/s. *Excluded as outlier from calculation of average. **This was the last value with decreasing MAE before the algorithm diverged.

value of η and the nominal value of L.

$$= \frac{2\pi(1.5 \times 10^{-2} Pa \cdot s)}{\ln\left(\frac{(1015.4 \times 10^{-6} m)}{(253.85 \times 10^{-6} m)}\right)}$$

$$= 0.0680$$

For the large aspect ratio cylinder we calculate:

$$k_t = \frac{2\pi(1.5 \times 10^{-2} Pa \cdot s)}{\ln\left(\frac{(2030.8 \times 10^{-6} m)}{(253.85 \times 10^{-6} m)}\right)}$$

$$= 0.0453$$

1.3 Cube Magnetization

We use the VSM to measure the magnetic moment of the magnets in each swimmer as described in Section 12. The magnetic moments, $\mathbf{m}_{cube}$, can be converted to magnetization per unit volume $\mathbf{M}_{cube}$ as follows (we use the mean magnetic moment measured for the nominal cylindrical swimmers as an example):

$$\mathbf{m}_{cube} = \mathbf{M}_{cube} V_{cube}$$

$$\mathbf{M}_{cube} = \frac{\mathbf{m}_{cube}}{V_{cube}}$$

$$= \frac{(7.44 \times 10^{-3} emu) \cdot \frac{10^{-3} A \cdot m^2}{emu}}{1.5625 \times 10^{-11} m^3}$$

$$= 476160 \frac{A}{m}$$

1.4 Link Masses

The mass of each link can be computed as the sum of the masses of the cured IP-S photoresin and the magnet (where appropriate). We assume that the mass of the nail polish and excess photoresist are negligible relative to the link mass and magnet mass. The density of cured IP-S photoresin is a conservative estimate based on experimental observations that solid links made of cured IP-S sank in water.

Let's first calculate the mass of the magnet. According to the manufacturer, the magnets are coated in a protective material that is $20\mu m$ thick on each side (so we subtract $40\mu m$ from the nominal side length of the cube). Furthermore, the manufacturer reports that magnets this small will see tooling damage during manufacturing that can reduce the total remanence by 50%. We can interpret this to mean that we should reduce the calculated volume of the magnet (after accounting for the coating) by a further 50%. The magnets are made of neodymium iron boron (NdFeB) and have a density of 7500 kg / m^3. Let's compute this mass:

$$m = \rho \cdot V$$

$$= 7500 \frac{kg}{m^3} \cdot 0.5 \left((0.00025m - 2(0.00002m))^3\right)$$

$$= 3.4729 \times 10^{-8} kg$$

Using this estimate of the magnet mass, we can compute the mass of link 1 for the nominal cylindrical swimmer as:

$$m_1 = m_{IP-S} + m_{magnet}$$

$$= \rho_{IP-S} \cdot V_{meas,1} + m_{magnet}$$

$$= (1200 kg/m^3)(0.0957 \times 10^{-9} m^3) + (3.4729 \times 10^{-8} kg)$$

$$= 1.4957 \times 10^{-7} kg$$

And for link 2:

$$m_2 = \rho_{IP-S} \cdot V_{meas,2}$$
$$= (1200 kg/m^3)(0.1220 \times 10^{-9} m^3)$$
$$= 1.464 \times 10^{-7} kg$$

For the large aspect ratio links, we start with link 1:

$$m_1 = (1200 kg/m^3)(0.3157 \times 10^{-9} m^3) + (3.4729 \times 10^{-8} kg)$$
$$= 4.1357 \times 10^{-7} kg$$

And for link 2:

$$m_2 = (1200 kg/m^3)(0.3637 \times 10^{-9} m^3)$$
$$= 4.3644 \times 10^{-7} kg$$

For the SF = 1.1 nominal swimmer, we start with link 1:

$$m_1 = (1200 kg/m^3)(0.1188 \times 10^{-9} m^3) + (3.4729 \times 10^{-8} kg)$$
$$= 1.7729 \times 10^{-7} kg$$

And for link 2:

$$m_2 = (1200 kg/m^3)(0.1448 \times 10^{-9} m^3)$$
$$= 1.7376 \times 10^{-7} kg$$

For the spherical links with equal diameters, we start with link 1:

$$m_1 = (1200 kg/m^3)(0.3157 \times 10^{-9} m^3) + (3.4729 \times 10^{-8} kg)$$
$$= 4.1357 \times 10^{-7} kg$$

And for link 2:

$$m_2 = (1200 kg/m^3)(0.3637 \times 10^{-9} m^3)$$
$$= 4.3644 \times 10^{-7} kg$$

For when link 2 is 75% the size of link 1, then we reduce the volume of link 2:

$$m_2 = (1200 kg/m^3)(0.1314 \times 10^{-9} m^3)$$
$$= 1.5768 \times 10^{-7} kg$$

1.5   Magnetic Field Parameters

In Section 10, we describe the details of how we measure the magnetic fields generated by our experimental setup. In the tables in this section, we report the values we calculated from that data, which we used in our models. Specifically, we report the value of B, b_x, b_y (see Section 2), as well as the duty cycle settings (duty$_x$ and duty$_y$) used to generate the $\mathbf{B_x}$ and $\mathbf{B_y}$ components with our Helmholtz coils.

1.6   Model Parameters

Description	Symbol	Value	Unit
Radius of swimmer joint	r	5×10^{-6}	m
Length of swimmer joint	L	39.5×10^{-6}	m
Torsion spring constant	κ	1.27×10^{-7}	$\frac{Nm}{rad}$
Length of link 1	L_1	1015.4×10^{-6}	m
Length of link 2	L_2	1015.4×10^{-6}	m
Radius of link 1	a_1	253.85×10^{-6}	m
Radius of link 2	a_2	253.85×10^{-6}	m
Hydrodynamic drag coefficient	k_t	0.325	$\frac{Ns}{m}$
Solid volume of link 1 (geometric)	V_1	$2.055611319 \times 10^{-10}$	m^3
Solid volume of link 2 (geometric)	V_2	$2.055611319 \times 10^{-10}$	m^3
Measured hollow volume of link 1 (from CAD)	$V_{meas,1}$	0.0957×10^{-9}	m^3
Measured hollow volume of link 2 (from CAD)	$V_{meas,2}$	0.1220×10^{-9}	m^3
Mass of link 1	m_1	1.50×10^{-7}	kg
Mass of link 2	m_2	1.46×10^{-7}	kg
Mean magnetic moment of cube	$\mathbf{m}_{cube}$	7.44×10^{-3}	emu
Mean magnetization per unit volume of cube	$\mathbf{M}_{cube}$	4.76×10^{5}	$A \cdot m^{-1}$

Table S5: Nominal cylindrical swimmer parameters. Parameters are reported to 3 significant figures when their corresponding calculations have been shown in the text; otherwise they are reported to additional significant figures for completeness.

Description	Symbol	Value	Unit
Radius of swimmer joint	r	5×10^{-6}	m
Length of swimmer joint	L	39.5×10^{-6}	m
Torsion spring constant	κ	1.27×10^{-7}	$\frac{Nm}{rad}$
Length of link 1	L_1	2030.8×10^{-6}	m
Length of link 2	L_2	2030.8×10^{-6}	m
Radius of link 1	a_1	253.85×10^{-6}	m
Radius of link 2	a_2	253.85×10^{-6}	m
Hydrodynamic drag coefficient	k_t	1.65	$\frac{Ns}{m}$
Solid volume of link 1 (geometric)	V_1	4.1112×10^{-10}	m^3
Solid volume of link 2 (geometric)	V_2	4.1112×10^{-10}	m^3
Measured hollow volume of link 1 (from CAD)	$V_{meas,1}$	0.2327×10^{-9}	m^3
Measured hollow volume of link 2 (from CAD)	$V_{meas,2}$	0.2678×10^{-9}	m^3
Mass of link 1	m_1	4.14×10^{-7}	kg
Mass of link 2	m_2	4.36×10^{-7}	kg
Mean magnetic moment of cube	$\mathbf{m}_{cube}$	9.34×10^{-3}	emu
Mean magnetization per unit volume of cube	$\mathbf{M}_{cube}$	5.98×10^5	$A \cdot m^{-1}$

Table S6: Large aspect ratio cylindrical swimmer parameters. Parameters are reported to 3 significant figures when their corresponding calculations have been shown in the text; otherwise they are reported to additional significant figures for completeness.

Description	Symbol	Value	Unit
Radius of swimmer joint	r	5×10^{-6}	m
Length of swimmer joint	L	79×10^{-6}	m
Torsion spring constant	κ	6.34×10^{-8}	$\frac{Nm}{rad}$
Length of link 1	L_1	1015.4×10^{-6}	m
Length of link 2	L_2	1015.4×10^{-6}	m
Radius of link 1	a_1	253.85×10^{-6}	m
Radius of link 2	a_2	253.85×10^{-6}	m
Hydrodynamic drag coefficient	k_t	0.288	$\frac{Ns}{m}$
Solid volume of link 1 (geometric)	V_1	$2.055611319 \times 10^{-10}$	m^3
Solid volume of link 2 (geometric)	V_2	$2.055611319 \times 10^{-10}$	m^3
Measured hollow volume of link 1 (from CAD)	$V_{meas,1}$	0.0957×10^{-9}	m^3
Measured hollow volume of link 2 (from CAD)	$V_{meas,2}$	0.1220×10^{-9}	m^3
Mass of link 1	m_1	1.50×10^{-7}	kg
Mass of link 2	m_2	1.46×10^{-7}	kg
Mean magnetic moment of cube	$\mathbf{m}_{cube}$	9.39×10^{-3}	emu
Mean magnetization per unit volume of cube	$\mathbf{M}_{cube}$	6.01×10^5	$A \cdot m^{-1}$

Table S7: Weak torsion spring cylindrical swimmer parameters. Parameters are reported to 3 significant figures when their corresponding calculations have been shown in the text; otherwise they are reported to additional significant figures for completeness.

Description	Symbol	Value	Unit
Radius of swimmer joint	r	5×10^{-6}	m
Length of swimmer joint	L	79×10^{-6}	m
Torsion spring constant	κ	1.27×10^{-7}	$\frac{\text{Nm}}{\text{rad}}$
Length of link 1	L_1	1015.4×10^{-6}	m
Length of link 2	L_2	1015.4×10^{-6}	m
Radius of link 1	a_1	253.85×10^{-6}	m
Radius of link 2	a_2	253.85×10^{-6}	m
Hydrodynamic drag coefficient (Percoll)	k_t	0.400	$\frac{Ns}{m}$
Hydrodynamic drag coefficient (Percoll/water)	k_t	0.353	$\frac{Ns}{m}$
Solid volume of link 1 (geometric)	V_1	$2.055611319 \times 10^{-10}$	m^3
Solid volume of link 2 (geometric)	V_2	$2.055611319 \times 10^{-10}$	m^3
Measured hollow volume of link 1 (from CAD)	$V_{meas,1}$	0.1188×10^{-9}	m^3
Measured hollow volume of link 2 (from CAD)	$V_{meas,2}$	0.1448×10^{-9}	m^3
Mass of link 1	m_1	1.77×10^{-7}	kg
Mass of link 2	m_2	1.74×10^{-7}	kg
Mean magnetic moment of cube	$\mathbf{m}_{cube}$	9.44×10^{-3}	emu
Mean magnetization per unit volume of cube	$\mathbf{M}_{cube}$	6.04×10^5	$A \cdot m^{-1}$
Dynamic viscosity of Percoll/water mixture	η	1.26×10^{-2}	$\frac{N}{m^2}s$

Table S8: SF = 1.1 cylindrical swimmer parameters. Parameters are reported to 3 significant figures when their corresponding calculations have been shown in the text; otherwise they are reported to additional significant figures for completeness.

Description	Symbol	Value	Unit
Radius of swimmer joint	r	5×10^{-6}	m
Length of swimmer joint	L	39.5×10^{-6}	m
Torsion spring constant	κ	1.27×10^{-7}	$\frac{\text{Nm}}{\text{rad}}$
Radius of link 1	L_1	507.7×10^{-6}	m
Radius of link 2	L_2	507.7×10^{-6}	m
Solid volume of link 1 (geometric)	V_1	5.4816×10^{-10}	m^3
Solid volume of link 2 (geometric)	V_2	5.4816×10^{-10}	m^3
Measured hollow volume of link 1 (from CAD)	$V_{meas,1}$	0.3157×10^{-9}	m^3
Measured hollow volume of link 2 (from CAD)	$V_{meas,2}$	0.3637×10^{-9}	m^3
Mass of link 1	m_1	4.14×10^{-7}	kg
Mass of link 2	m_2	4.36×10^{-7}	kg
Mean magnetic moment of cube	$\mathbf{m}_{cube}$	5.86×10^{-3}	emu
Mean magnetization per unit volume of cube	$\mathbf{M}_{cube}$	3.75×10^5	$A \cdot m^{-1}$

Table S9: Nominal spherical swimmer parameters. Parameters are reported to 3 significant figures when their corresponding calculations have been shown in the text; otherwise they are reported to additional significant figures for completeness.

Description	Symbol	Value	Unit
Radius of swimmer joint	r	5×10^{-6}	m
Length of swimmer joint	L	39.5×10^{-6}	m
Torsion spring constant	κ	1.27×10^{-7}	$\frac{Nm}{rad}$
Radius of link 1	L_1	507.7×10^{-6}	m
Radius of link 2	L_2	380.775×10^{-6}	m
Solid volume of link 1 (geometric)	V_1	5.4816×10^{-10}	m^3
Solid volume of link 2 (geometric)	V_2	2.3126×10^{-10}	m^3
Measured hollow volume of link 1 (from CAD)	$V_{meas,1}$	0.3157×10^{-9}	m^3
Measured hollow volume of link 2 (from CAD)	$V_{meas,2}$	0.3637×10^{-9}	m^3
Mass of link 1	m_1	4.14×10^{-7}	kg
Mass of link 2	m_2	1.58×10^{-7}	kg
Mean magnetic moment of cube	$\mathbf{m}_{cube}$	9.07×10^{-3}	emu
Mean magnetization per unit volume of cube	$\mathbf{M}_{cube}$	5.80×10^5	$A \cdot m^{-1}$

Table S10: $\alpha = 0.75$ spherical swimmer parameters. Parameters are reported to 3 significant figures when their corresponding calculations have been shown in the text; otherwise they are reported to additional significant figures for completeness.

Description	Symbol	Value	Unit
Young's modulus of cured IP-S photoresin	E	5.1×10^9	$\frac{N}{m^2}$
Dynamic viscosity of Percoll	η	1.5×10^{-2}	$\frac{N}{m^2}s$
Length of magnetic cube	L_{cube}	250×10^{-6}	m
Mass of magnetic cube	m_{cube}	3.47×10^{-8}	kg
Volume of magnetic cube	V_{cube}	1.5625×10^{-11}	m^3
Density of cured IP-S photoresin	ρ_{IP-S}	1200	$kg \cdot m^{-3}$
Residual mass of glue, nail polish	$m_{residual}$	3.733×10^{-8}	kg

Table S11: Shared model parameters. Parameters are reported to 3 significant figures when their corresponding calculations have been shown in the text; otherwise they are reported to additional significant figures for completeness.

Description	Symbol	Value	Unit
Magnitude of magnetic field	B	0.000413152794447071	T
Fraction of B in x direction	b_x	0.8669903867	[]
Fraction of B in y direction	b_y	1	[]
Magnitude of duty cycle in x direction	duty_x	0.1	[]
Magnitude of duty cycle in y direction	duty_y	0.05	[]

Table S12: Magnetic field parameters for $\beta = 1$, B_x^+ case. Parameters are reported to 3 significant figures when their corresponding calculations have been shown in the text; otherwise they are reported to additional significant figures for completeness.

Description	Symbol	Value	Unit
Magnitude of magnetic field	B	0.000337250816259859	T
Fraction of B in x direction	b_x	-1.042404471	[]
Fraction of B in y direction	b_y	1	[]
Magnitude of duty cycle in x direction	duty_x	0.1	[]
Magnitude of duty cycle in y direction	duty_y	0.04	[]

Table S13: Magnetic field parameters for $\beta = 1$, B_x^- case. Parameters are reported to 3 significant figures when their corresponding calculations have been shown in the text; otherwise they are reported to additional significant figures for completeness.

Description	Symbol	Value	Unit
Magnitude of magnetic field	B	0.000678705694902381	T
Fraction of B in x direction	b_x	0.5226617093	[]
Fraction of B in y direction	b_y	1	[]
Magnitude of duty cycle in x direction	duty_x	0.1	[]
Magnitude of duty cycle in y direction	duty_y	0.08	[]

Table S14: Magnetic field parameters for $\beta = 2$, B_x^+ case. Parameters are reported to 3 significant figures when their corresponding calculations have been shown in the text; otherwise they are reported to additional significant figures for completeness.

Description	Symbol	Value	Unit
Magnitude of magnetic field	B	0.00067847052983757	T
Fraction of B in x direction	b_x	-0.5153961541	[]
Fraction of B in y direction	b_y	1	[]
Magnitude of duty cycle in x direction	duty_x	0.1	[]
Magnitude of duty cycle in y direction	duty_y	0.08	[]

Table S15: Magnetic field parameters for $\beta = 2$, B_x^- case. Parameters are reported to 3 significant figures when their corresponding calculations have been shown in the text; otherwise they are reported to additional significant figures for completeness.

Description	Symbol	Value	Unit
Magnitude of magnetic field	B	0.00124161749346226	T
Fraction of B in x direction	b_x	0.3438480027	[]
Fraction of B in y direction	b_y	1	[]
Magnitude of duty cycle in x direction	duty_x	0.1	[]
Magnitude of duty cycle in y direction	duty_y	0.15	[]

Table S16: Magnetic field parameters for $\beta = 3$, B_x^+ case. Parameters are reported to 3 significant figures when their corresponding calculations have been shown in the text; otherwise they are reported to additional significant figures for completeness.

Description	Symbol	Value	Unit
Magnitude of magnetic field	B	0.00103159297212759	T
Fraction of B in x direction	b_x	-0.335591789	[]
Fraction of B in y direction	b_y	1	[]
Magnitude of duty cycle in x direction	$duty_x$	0.1	[]
Magnitude of duty cycle in y direction	$duty_y$	0.12	[]

Table S17: Magnetic field parameters for $\beta = 3$, B_x^- case. Parameters are reported to 3 significant figures when their corresponding calculations have been shown in the text; otherwise they are reported to additional significant figures for completeness.

1.7 Parameters for Buoyancy Test

In this section we describe the calculations used to estimate the model parameters for our buoyancy test with a cylindrical swimmer with safety factor of 1.1.

We can compute the approximate dynamic viscosity of a mixture of water and Percoll as a weighted average. We know that we used 1.2mL of water and 6mL of Percoll so:

$$\eta_{\text{mixture}} = \frac{1.2mL}{7.2mL}(8.891 \times 10^{-4} Pa \cdot s) + \frac{6mL}{7.2mL}(1.5 \times 10^{-2} Pa \cdot s)$$
$$= 1.264818333 \times 10^{-2} Pa \cdot s$$

The mass of link 1 is:

$$m_1 = m_{IP-S} + m_{magnet}$$
$$= \rho_{IP-S} \cdot V_{meas,1} + m_{magnet}$$
$$= (1200 kg/m^3)(0.1188 \times 10^{-9} m^3) + (3.4729 \times 10^{-8} kg)$$
$$= 1.7729 \times 10^{-7} kg$$

And for link 2:

$$m_2 = \rho_{IP-S} \cdot V_{meas,2}$$
$$= (1200 kg/m^3)(0.1448 \times 10^{-9} m^3)$$
$$= 1.7376 \times 10^{-7} kg$$

2 Detailed Model Derivation

2.1 Cylindrical Links

This model represents the swimmer links as cylinders connected by a torsion spring. As shown in Figure 2A in the main text, we can use the center of mass of the first link, point $\mathbf{p_1} = [x_1, y_1]$, and the angle of each link written with respect to the inertial frame to completely describe the swimmer's configuration, that is: $[x_1, y_1, \theta_1, \theta_2] \in \mathbb{R}$.

To derive the equations of motion for this system, we can balance the forces and torques that act on this swimmer, as shown in Figure 2B in the main paper. The corresponding equations of motion are:

$$\mathbf{F_{1,h}} + \mathbf{F_{2,h}} = \mathbf{0} \tag{S1}$$
$$-\tau_{1,h}^{\mathbf{p_1}} + \tau_{2,h}^{\mathbf{p_1}} + \tau_{1,m} = \mathbf{0} \tag{S2}$$
$$\tau_{2,h}^{\mathbf{p_2}} + \tau_{\kappa,2} = \mathbf{0} \tag{S3}$$

Equation S1 is a sum of the forces acting on the entire system, and Equation S2 is the sum of the torques acting on the entire system. In order to solve for the final state variable, we also write Equation S3, which is the sum of the torques acting on link 2, specifically.

The forces $\mathbf{F_{i,h}}$ are the hydrodynamic drag forces acting on the i-th link with respect to the inertial frame's x- and y-axes. The torques due to hydrodynamic drag are written as $\tau_{\mathbf{i,h}}^{\mathbf{p_j}}$, where the torque is acting on link i and written with respect to point p_j. The torque due to magnetic misalignment and acting on link 1 is $\tau_{\mathbf{1,m}}$. The torque produced by the torsion spring and acting on link 2 is $\tau_{\kappa,\mathbf{2}}$. Notice that the sum of the forces and torques in each direction are equal to zero because we assume that our milliswimmer is small enough to be in a low Reynolds number regime and therefore the dynamics are quasistatic (i.e. the milliswimmer has no inertia). We will work through each equation in more detail below.

First, we define the transverse and normal vectors for each link.

$$\hat{\mathbf{t}}_1 = [\cos(\theta_1), \sin(\theta_1)]^T$$
$$\hat{\mathbf{n}}_1 = [-\sin(\theta_1), \cos(\theta_1)]^T$$
$$\hat{\mathbf{t}}_2 = [\cos(\theta_2), \sin(\theta_2)]^T$$
$$\hat{\mathbf{n}}_2 = [-\sin(\theta_2), \cos(\theta_2)]^T$$

We can write the position and velocity vectors for the center of mass of each link as:

$$\mathbf{p_1} = [x_1, y_1]$$
$$\dot{\mathbf{p}}_1 = [\dot{x}_1, \dot{y}_1]$$
$$\mathbf{p_2} = \mathbf{p_1} + \frac{L_1}{2}\hat{\mathbf{t}}_1 + \frac{L_2}{2}\hat{\mathbf{t}}_2$$
$$\dot{\mathbf{p}}_2 = \dot{\mathbf{p}}_1 + \frac{L_1}{2}\hat{\mathbf{n}}_1\dot{\theta}_1 + \frac{L_2}{2}\hat{\mathbf{n}}_2\dot{\theta}_2$$

2.1.1 Hydrodynamic Forces

To write the hydrodynamic forces acting on each link, we can write the force per unit length on the ith link as:

$$\mathbf{f_{i,h}}(s) = -k_t\langle\dot{\mathbf{p}}_\mathbf{i}(s), \hat{\mathbf{t}}_\mathbf{i}\rangle\hat{\mathbf{t}}_\mathbf{i} - 2k_t\langle\dot{\mathbf{p}}_\mathbf{i}(s), \hat{\mathbf{n}}_\mathbf{i}\rangle\hat{\mathbf{n}}_\mathbf{i}$$

Where s is the variable of integration from $s = [-0.5, 0.5]$ along the length of the link with the origin at the center of mass of the link. The position $\mathbf{p_i}(s)$ can be written as $\mathbf{p_i} + sL_i\hat{\mathbf{t}}_\mathbf{i}$, and the velocity $\dot{\mathbf{p}}_\mathbf{i}(s)$ can be written as $\dot{\mathbf{p}}_\mathbf{i} + sL_i\hat{\mathbf{n}}_\mathbf{i}\dot{\theta}_i$. We can define k_t as the drag coefficient for a cylinder per [2, 3, 4], $k_t = \frac{2\pi\eta}{\ln(L/a)}$, where η is the dynamic viscosity of the fluid, L is the length and a is the radius of the cylinder. (When we move to a second order system, we will use a different value of k_t estimated from the experimental data - see Section 1.2 for a detailed discussion on this point.) To compute the hydrodynamic drag forces, we integrate $\mathbf{f_{i,h}}(s)$ with respect to s:

$$\begin{aligned}
\mathbf{F_{i,h}} &= \int_{-0.5}^{0.5} \mathbf{f_{i,h}}(s)\big(L_i(s+ds) - L_i s\big) \\
&= \int_{-0.5}^{0.5} L_i \cdot \mathbf{f_{i,h}}(s)\, ds \\
&= -k_t L_i \int_{-0.5}^{0.5} \langle\dot{\mathbf{p}}_\mathbf{i}(s), \hat{\mathbf{t}}_\mathbf{i}\rangle\hat{\mathbf{t}}_\mathbf{i} + 2\langle\dot{\mathbf{p}}_\mathbf{i}(s), \hat{\mathbf{n}}_\mathbf{i}\rangle\hat{\mathbf{n}}_\mathbf{i}\, ds
\end{aligned}$$

2.1.2 Hydrodynamic Torques

We now can derive similar equations for the hydrodynamic torques acting on the links. In general, we can write the hydrodynamic torque per unit length acting on link i about the point j as:

$$\tau_{\mathbf{i,h}}^{\mathbf{p_j}}(s) = (\mathbf{p_i}(s) - \mathbf{p_j}) \times \mathbf{f_{i,h}}(s)$$

Then we can integrate the torque per unit length as follows:

$$\tau_{\mathbf{i,h}}^{\mathbf{pj}} = \int_{-0.5}^{0.5} \tau_{\mathbf{i,h}}^{\mathbf{pj}}(s)(L_i(s+ds) - L_i s)$$

$$= \int_{-0.5}^{0.5} L_i \cdot \tau_{\mathbf{i,h}}^{\mathbf{pj}}(s)\, ds$$

$$= k_t L_i \int_{-0.5}^{0.5} (\mathbf{p_i}(s) - \mathbf{p_j}) \times \left(- \langle \dot{\mathbf{p}}_i(s), \hat{\mathbf{t}}_i \rangle \hat{\mathbf{t}}_i - 2\langle \dot{\mathbf{p}}_i(s), \hat{\mathbf{n}}_i \rangle \hat{\mathbf{n}}_i \right) ds$$

2.1.3 Magnetic and Spring Torques

Finally, the torque due to misalignment between the magnetic links and the external magnetic field can be written as:

$$\tau_{\mathbf{1,m}} = V_1 \mathbf{M_1} \times \mathbf{B}(\omega, t)$$

Where $\mathbf{M_1} = (m_{1,t}\hat{\mathbf{t}}_1 + m_{1,n}\hat{\mathbf{n}}_1)$. We will rewrite the magnetization vector $\mathbf{M_1}$ to separate out the magnitude from the directions in which it is acting as follows:

$$\mathbf{M_1} = m(h_{1,t}\hat{\mathbf{t}}_1 + h_{1,n}\hat{\mathbf{n}}_1)$$

Where $h_{1,t}, h_{1,n} \in [0,1]$ and m is the magnitude of the link's magnetization. Similarly, we can rewrite the $\mathbf{B}(\omega, t)$ term to separate the magnitude of the magnetic field from its directionality as follows:

$$\mathbf{B}(\omega, \mathbf{t}) = B[b_x(\omega, t), b_y(\omega, t)]^T$$

Where $b_x(\omega, t), b_y(\omega, t) \in [0,1]$, and B is the magnitude of the field. Finally, we can write the spring torque as $\tau_{\kappa,\mathbf{i}} = \kappa(\theta_2 - \theta_1)$, where κ is the torsion spring constant.

We can now combine the torques to write Equation S2:

$$-\tau_{\mathbf{1,h}}^{\mathbf{p1}} + \tau_{\mathbf{2,h}}^{\mathbf{p1}} + \tau_{\mathbf{1,m}} = - k_t L \int_{-0.5}^{0.5} \tau_{\mathbf{1,h}}^{\mathbf{p1}}(s)\, ds$$

$$+ k_t \alpha L \int_{-0.5}^{0.5} \tau_{\mathbf{2,h}}^{\mathbf{p1}}(s)\, ds$$

$$+ V_1 m(h_{1,t}\hat{\mathbf{t}}_1 + h_{1,n}\hat{\mathbf{n}}_1) \times B[b_x(\omega, t), b_y(\omega, t)]^T$$

Finally, we can rewrite Equation S3:

$$\tau_{\mathbf{2,h}}^{\mathbf{p2}} + \tau_{\kappa,\mathbf{2}} = k_t L_2 \int_{-0.5}^{0.5} \tau_{\mathbf{2,h}}^{\mathbf{p2}}(s)\, ds + V_2 m B \left((h_{2,t}\hat{\mathbf{t}}_2 + h_{2,n}\hat{\mathbf{n}}_2) \times [b_x(\omega, t), b_y(\omega, t)]^T \right) + \kappa(\theta_2 - \theta_1)$$

2.1.4 Defining the Swimmer Centroid

We define the centroid of the milliswimmer as the point at which the first and second links join together. We will use this centroid as a reference point from which to measure the milliswimmer's trajectories and translational velocities. This allows us to directly compare our model predictions to our experimental findings, where we are also tracking the position of our experimental swimmers with respect to their centroid. Our model as written above returns the position and translational velocity of the center of link 1, and we convert to the centroid using the following expressions:

$$\begin{bmatrix} x_c \\ y_c \end{bmatrix} = \begin{bmatrix} x_1 \\ y_1 \end{bmatrix} + \frac{L_1}{2}\hat{\mathbf{t}}_1$$

$$\begin{bmatrix} \dot{x}_c \\ \dot{y}_c \end{bmatrix} = \begin{bmatrix} \dot{x}_1 \\ \dot{y}_1 \end{bmatrix} + \frac{L_1}{2}\hat{\mathbf{n}}_1 \dot{\theta}_1$$

2.2 Spherical Links

Now we present a modification to the milliswimmer model that changes the shape of the links from cylinders to spheres. The coordinate system for the spherical model is the same as that used in the cylindrical model, with adjustments made for the fact that the link dimension is represented by the radius of the spheres instead of the length of the cylinders. We also change the representation of the angles of the two links to be θ for link 1 and α for link 2, where α is measured with respect to link 1. This change makes writing the equations for the torques acting on each link more straightforward. The coordinate system is shown in Figure 2C in the main paper.

As before, our modeling approach is to compute the sum of the forces and torques acting on the entire system, as well as the torques acting on the second link, to obtain expressions for each position variable (x, y), and each joint angle, (θ, α), in the system, as described in Equations S1-S3. The free body diagram for our system is shown in Figure 2D in the main paper.

With our new definition of the angles for this system, we can define the transverse and normal vectors for each link.

$$\hat{\mathbf{t}}_1 = [\cos(\theta), \sin(\theta)]^T$$
$$\hat{\mathbf{n}}_1 = [-\sin(\theta), \cos(\theta)]^T$$
$$\hat{\mathbf{t}}_2 = [\cos(\theta + \alpha), \sin(\theta + \alpha)]^T$$
$$\hat{\mathbf{n}}_2 = [-\sin(\theta + \alpha), \cos(\theta + \alpha)]^T$$

We present the derivation of the expression for each of the forces and torques below.

2.2.1 Hydrodynamic Forces

In this low Reynolds number environment, we can write the hydrodynamic drag force acting on each spherical link as $\mathbf{F}_{\mathbf{i,h}} = -6\pi\eta r_i \dot{\mathbf{p}}_{\mathbf{i}}$ [5], giving Equation S1 for this system as:

$$\mathbf{F}_{\mathbf{1,h}} + \mathbf{F}_{\mathbf{2,h}} = \mathbf{0}$$
$$-6\pi\eta r_1 \dot{\mathbf{p}}_{\mathbf{1}} - 6\pi\eta r_2 \dot{\mathbf{p}}_{\mathbf{2}} = \mathbf{0}$$

2.2.2 Hydrodynamic, Magnetic and Torsion Spring Torques

Similarly, under the same conditions, the torque due to hydrodynamic (or viscous) drag on a spherical link, acting about the center of mass of that link, can be written as $\tau_{\mathbf{i,h}} = 8\pi\eta r_i^3 \Omega_i$ where Ω_i represents the rotational velocity of the i-th link [5]. For the torque acting on link 2 but written with respect to the center of link 1, the expression is $\tau_{\mathbf{2,h}}^{\mathbf{p1}} = 8\pi\eta(r_2)^3(\dot{\theta} + \dot{\alpha}) + 6\pi\eta r_2(\mathbf{r}_{\mathbf{1}\rightarrow\mathbf{2}})^2\dot{\theta}$, where $\mathbf{r}_{\mathbf{1}\rightarrow\mathbf{2}}$ is the vector from the center of link 1 to the center of link 2 [6]. According to [6], the first term is the torque due to the rotation of the sphere about its own center of mass, and the second term is caused by translation of the sphere's center of mass through the fluid about some point other than its own center of mass.

The torque due to misalignment between the magnetic links and the external magnetic field can be written as $\tau_{\mathbf{i,m}} = V_i \mathbf{M}_{\mathbf{i}} \times \mathbf{B}(\omega, t)$ where $\mathbf{M}_{\mathbf{i}} = (m_{i,t}\hat{\mathbf{t}}_{\mathbf{i}} + m_{i,n}\hat{\mathbf{n}}_{\mathbf{i}})$ and $\mathbf{B}(\omega, t) = [B_x(\omega, t), B_y(\omega, t)]^T$. As before, we can rewrite both of these to separate the direction of the vector from its magnitude. Given this, we can write Equation S2 for this system as:

$$-\tau_{\mathbf{1,h}}^{\mathbf{p1}} + \tau_{\mathbf{2,h}}^{\mathbf{p1}} + \tau_{\mathbf{1,m}} = -8\pi\eta r_1^3\dot{\theta}$$
$$+ \left(8\pi\eta r_2^3(\dot{\theta} + \dot{\alpha}) + 6\pi\eta r_2(\mathbf{r}_{\mathbf{1}\rightarrow\mathbf{2}})^2\dot{\theta}\right)$$
$$+ V_1 m(h_{1,t}\hat{\mathbf{t}}_{\mathbf{1}} + h_{1,n}\hat{\mathbf{n}}_{\mathbf{1}}) \times B[b_x(\omega, t), b_y(\omega, t)]^T$$

And finally, the torque due to the torsion spring can be written as $\tau_{\kappa,\mathbf{i}} = \kappa\alpha$. Then we can write Equation S3 for this system as:

$$\tau_{\mathbf{2,h}}^{\mathbf{p2}} + \tau_{\kappa,\mathbf{2}} = 8\pi\eta r_2^3(\dot{\theta} + \dot{\alpha}) + \kappa\alpha$$

17

2.3 Writing the Dynamics as a Second-Order System

As we show in the main paper results, we found that the first order model predictions for our spherical swimmers did not match the experimental results well. Specifically, our first order model predicted that the spherical swimmer with dissimilar link diameters would have negligible velocity, but we found that those swimmers actually exhibited a velocity on the same order of magnitude as our cylindrical links.

Our first order model assumes that the milliswimmers are quasi-static, which is true when we consider the net velocity of the milliswimmer, but when we consider their instantaneous velocities, we can see that they display higher Reynolds numbers. This may suggest that we need to incorporate second-order effects like momentum into our model. Let's begin by computing the Reynolds number for the milliswimmer using the net velocity we observe experimentally.

$$
\begin{aligned}
Re &= \frac{\rho v L}{\mu} \\
&= \frac{(1130\text{kg/m}^3)(1 \times 10^{-5}\text{m/s})(1015 \times 10^{-6}\text{m})}{(1.5 \times 10^{-2}\text{kg/m} \cdot \text{s})} \\
&= 0.000765
\end{aligned}
$$

However, if we compute the instantaneous velocity of a swimmer as it sweeps through an oscillation from $-45°$ to $+45°$, then the instantaneous velocity for 1Hz is:

$$
\begin{aligned}
v_{instant} &= \frac{\text{arc length}}{\text{time}} \\
&= \frac{90° \left(\frac{\pi}{180°}\right)(507 \times 10^{-6}\text{m})}{0.5\text{s}} \\
&= 0.00159\text{m/s}
\end{aligned}
$$

This instantaneous velocity at 1Hz is 2 orders of magnitude larger than the net velocity of the swimmer. And for a 10Hz oscillation the instantaneous velocity is ten times this value, 0.0159m/s, which is 3 orders of magnitude larger than the swimmer's net velocity.

Given these velocities, we can calculate the following Reynolds numbers for the instantaneous motion at 1Hz and 10Hz:

$$
Re_{1Hz} = 0.122
$$
$$
Re_{10Hz} = 1.22
$$

Correspondingly, the Reynolds numbers for the swimmers when considering instantaneous velocity are 3-4 orders of magnitude larger than the Reynolds number when considering the swimmer's net velocity. This suggests that the quasi-static assumption no longer holds, and we need to consider the second order dynamics.

For $\beta = 3$ we estimate that the swimmer now sweeps through $-80°$ to $+80°$, leading to an instantaneous velocity at 1Hz of:

$$
\begin{aligned}
v_{instant} &= \frac{160° \left(\frac{\pi}{180°}\right)(507 \times 10^{-6}m)}{0.5s} \\
&= 0.0032\text{m/s}
\end{aligned}
$$

And for 10Hz the instantaneous velocity is 0.0319m/s. Then the corresponding Reynolds numbers are 0.245 and 2.44, respectively.

Accordingly, we can rewrite the equations of motion for the cylindrical two-link swimmer model as:

$$
m_1 \ddot{\mathbf{p}}_1 = \mathbf{F}_{1,\mathbf{h}} \tag{S4}
$$
$$
m_2 \ddot{\mathbf{p}}_2 = \mathbf{F}_{2,\mathbf{h}} \tag{S5}
$$
$$
I_1 \ddot{\theta}_1 = -\tau_{1,\mathbf{h}}^{\mathbf{p},1} - \tau_{\kappa,1} + \tau_{1,\mathbf{m}} \tag{S6}
$$
$$
-I_2 \ddot{\theta}_2 = \tau_{2,\mathbf{h}}^{\mathbf{p},2} + \tau_{\kappa,2} \tag{S7}
$$

Here m_1 and m_2 are the mass of link 1 and link 2, respectively. The accelerations of each link are written as $\ddot{\mathbf{p}}_1$ and $\ddot{\mathbf{p}}_2$ and the angular accelerations are $\ddot{\theta}_1$ and $\ddot{\theta}_2$. The moment of inertia for the i-th link about the i-th point p_i is I_i.

Similarly, we can write the spherical model as follows:

$$m_1\ddot{\mathbf{p}}_1 = \mathbf{F}_{1,\mathbf{h}} \tag{S8}$$

$$m_2\ddot{\mathbf{p}}_2 = \mathbf{F}_{2,\mathbf{h}} \tag{S9}$$

$$I_1\ddot{\theta} = -\tau_{1,\mathbf{h}}^{\mathbf{p_1}} - \tau_{\kappa,1} + \tau_{1,\mathbf{m}} \tag{S10}$$

$$-I_2(\ddot{\theta} + \ddot{\alpha}) = \tau_{2,\mathbf{h}}^{\mathbf{p_2}} + \tau_{\kappa,2} \tag{S11}$$

2.3.1 Including Magnetic Field Gradient in Second Order Model

We also hypothesized that the small, nonzero magnetic field gradient present in our workspace may be affecting our experimental results, so we wrote another version of our second order model that included the force applied by the magnetic field gradient to the magnetic link 1. Specifically, Equations S4 and S8 are modified to include a term for the force applied by the magnetic field gradient:

$$m_1\ddot{\mathbf{p}}_1 = \mathbf{F}_{1,\mathbf{h}} + \mathbf{F}_{\nabla\mathbf{B}}$$

We can write the force due to the magnetic field gradient as:

$$\mathbf{F}_{\nabla\mathbf{B}} = V_i\mathbf{M_i} \cdot \nabla\mathbf{B}$$
$$= V_i m(h_{i,t}\hat{\mathbf{t}}_\mathbf{i} + h_{i,n}\hat{\mathbf{n}}_\mathbf{i}) \cdot (\nabla B_x, \nabla B_y)$$

In the next section we will present a derivation of the magnetic field gradient that we use to obtain the values of $\nabla\mathbf{B} = (\nabla B_x, \nabla B_y)$.

3   Model of Helmholtz Coil Magnetic Field Gradients

This section describes the derivation of the magnetic field and the magnetic field gradient for a coil of wire. This method will allow us to write the value of the field and the gradient anywhere in space, and is based upon work presented in [7, 8].

3.1   Magnetic Field

We start with the vector potential, A, for a magnetic field produced by a circular wire carrying a current, I [7, 8].

$$\mathbf{A}(r) = \frac{\mu_0 I}{4\pi} \int \frac{d\mathbf{l}}{|\mathbf{r} - \mathbf{r'}|}$$
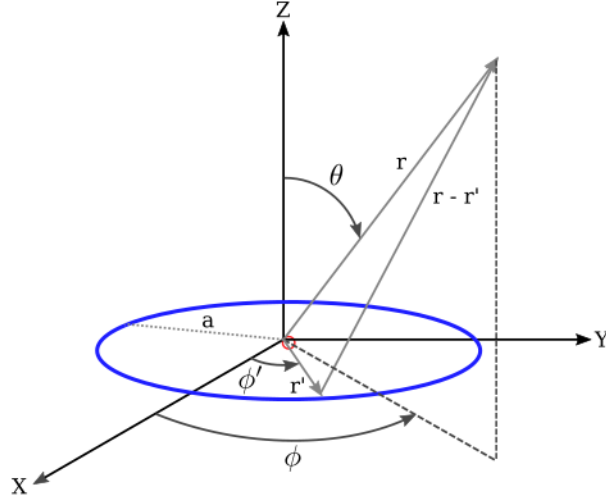
Figure S1: Coil model.

Note that in general, the vector field $\mathbf{A}(r)$ is the same for every value of φ because it is symmetric about the axis z. In this case, we can arbitrarily set $\varphi = 0$ to simplify the system.

As shown in Figure S1, when $\varphi = 0$, the value of $\mathbf{A}$ at an arbitrary point described by the vector $\mathbf{r}$ is a function of the radial distances in the x-y ($\mathbf{r}'$) and y-z planes ($\mathbf{r}$), as well as the current, I and a differential element of the arc length of the coil segment, $d\mathbf{l}$.

We can write the vectors as follows:

$$d\mathbf{l} = (-asin\varphi', acos\varphi', 0)d\varphi' \tag{S12}$$

$$\mathbf{r} = (rsin\theta, 0, rcos\theta) \tag{S13}$$

$$\mathbf{r'} = (acos\varphi', asin\varphi', 0) \tag{S14}$$

$$|\mathbf{r} - \mathbf{r'}| = \sqrt{(rsin\theta - acos\varphi')^2 + (r^2cos^2\theta) + (a^2sin^2\varphi')} \tag{S15}$$

Equation S15 simplifies to:

$$|\mathbf{r} - \mathbf{r'}| = \sqrt{r^2 + a^2 - 2rasin\theta cos\varphi'}$$

Now we rewrite the expression for $\mathbf{A}$:

$$\mathbf{A}(r, \theta) = \frac{\mu_0 I}{4\pi} \cdot 2 \cdot \int_0^\pi \frac{acos\varphi' d\varphi'}{\sqrt{r^2 + a^2 - 2rasin\theta cos\varphi'}}$$

Notice that the $-asin\varphi'$ term in $d\mathbf{l}$ is removed because it is odd so when it integrates, it integrates to 1. Now this expression is converted to cylindrical coordinates, (ρ, φ, z). Specifically, we observe that $\mathbf{r} = (\rho, 0, \mathbf{z})$. Thus we obtain:

$$\mathbf{A}(\rho, z) = \frac{\mu_0 I}{2\pi} \int_0^\pi \frac{acos\varphi' d\varphi'}{\sqrt{\rho^2 + z^2 + a^2 - 2a\rho cos\varphi'}}$$

This integral does not have a closed form solution. Instead, we are going to use a change of variables and a substitution to write the vector field as a function of elliptic integrals which we can solve numerically. First, let $\varphi' = \pi + 2\phi$:

$$\mathbf{A}(\rho, z) = \frac{\mu_0 I a}{\pi} \int_0^{\frac{\pi}{2}} \frac{(2sin^2\phi - 1)d\phi}{\sqrt{(a+\rho)^2 + z^2 - 4a\rho sin^2\phi}}$$

And we write some of these terms into a single variable, k:

$$k^2 = \frac{4a\rho}{(a+\rho)^2 + z^2}$$

20

Now the integral becomes:

$$\mathbf{A}(\rho,\phi) = \frac{\mu_0 I}{\pi k}\sqrt{\frac{a}{\rho}}\left[(1-\frac{k^2}{2})K(k) - E(k)\right] \text{ where}$$

$$K(k) = \int_0^{\frac{\pi}{2}} \frac{d\phi}{\sqrt{1-k^2 sin^2\phi}}$$

$$E(k) = \int_0^{\frac{\pi}{2}} \sqrt{1-k^2 sin^2\phi}\, d\phi$$

$K(k)$ is the complete elliptic integral of the first kind, and $E(k)$ is the complete elliptic integral of the second kind. They were originally derived for the purposes of calculating the arc length of an ellipse. The key fact about these integrals, for our purposes, is that they are numerically solvable.

Now we obtain the final expressions for the magnetic field in the ρ and z directions by using the curl of $\mathbf{A}$, written in terms of cylindrical coordinates:

$$\mathbf{B} = \nabla \times \mathbf{A}$$

$$B_\rho(\rho,z) = -\frac{\partial A_\phi}{\partial z}$$

$$B_z(\rho,z) = \frac{1}{\rho}\frac{\partial}{\partial\rho}(\rho A_\phi)$$

Note that we are concerned with the field in the ρ and z directions because the field will have the same value for all ϕ since the vector field is symmetric along that direction. We will need the derivatives of the elliptic integrals and of k with respect to z and ρ as follows:

$$\frac{\partial K}{\partial k} = \frac{E}{k(1-k^2)} - \frac{K}{k}$$

$$\frac{\partial E}{\partial k} = \frac{E}{k} - \frac{K}{k}$$

$$\frac{\partial k}{\partial\rho} = \frac{k}{2\rho} - \frac{k^3}{4\rho} - \frac{k^3}{4a}$$

$$\frac{\partial k}{\partial z} = -\frac{zk^3}{4a\rho}$$

We can use the chain rule to combine these derivatives together. Finally, after some manipulation, our expressions are:

$$B_\rho(\rho,z) = \frac{\mu_0 n I}{2\pi}\frac{z}{\rho\sqrt{(\rho+a)^2+z^2}}\left[\frac{a^2+\rho^2+z^2}{(a-\rho)^2+z^2}E(k) - K(k)\right] \tag{S16}$$

$$B_z(\rho,z) = \frac{\mu_0 n I}{2\pi}\frac{1}{\sqrt{(\rho+a)^2+z^2}}\left[\frac{a^2-\rho^2-z^2}{(a-\rho)^2+z^2}E(k) + K(k)\right] \tag{S17}$$

Note that the numerator includes the term n to account for multiple turns of wire in the coils. Then we can add the influence of multiple coils together, for the Helmholtz coil configuration, as follows:

$$B_\rho^{total}(\rho,z) = B_\rho(\rho,z+d) + B_\rho(\rho,z-d) \tag{S18}$$

$$B_z^{total}(\rho,z) = B_z(\rho,z+d) + B_z(\rho,z-d) \tag{S19}$$

Where d is the separation between the coils. For Helmholtz coils, $d = \frac{r}{2}$ where r is the radius of the coils.

Now that we have expressions for the magnetic field in the ρ and z directions (Equations S16 and S17), we can calculate the magnitude of the net magnetic field at any point in space as the Euclidean sum of the two components, which are vectors of B in the corresponding directions ρ and z:

$$|\mathbf{B}| = \sqrt{\mathbf{B}_\rho^2 + \mathbf{B}_z^2} \tag{S20}$$

We can check this model by comparing the simulated values as obtained above with the analytic solution to the field in the z-direction along the centerline of a pair of Helmholtz coils (this is the Biot-Savart Law):

$$B_z = \frac{0.5\mu_0 a^2 I}{\sqrt{(a^2 + z^2)^3}} \tag{S21}$$

Therefore, the first check we perform is to plot the magnetic field along the centerline between the two axes as obtained via our Equations S18 and S19 above and compare it to the solution obtained via the analytical expression in Equation S21. We do this for both of our sets of coils (distinguished by their manufacturer, 3B and Pasco), for maximum current values used when $\beta = 1.5$. This is shown in Figure S2. The dashed red line indicates the magnitude of the field along the centerline as calculated by our model in Equations S18 and S19. The magenta and green lines plot the magnetic field generated by each coil in the pair individually, as calculated using the Biot-Savart Law in Equation S21. The dashed black line is the sum of these two individual fields, and it shows agreement with the dashed red line that represents our more complex model. Similarly, the result of calculating the Biot-Savart Law for both coils together, as shown in the solid blue line, also shows close agreement with the sum of the individual coils' fields and the more complex model.
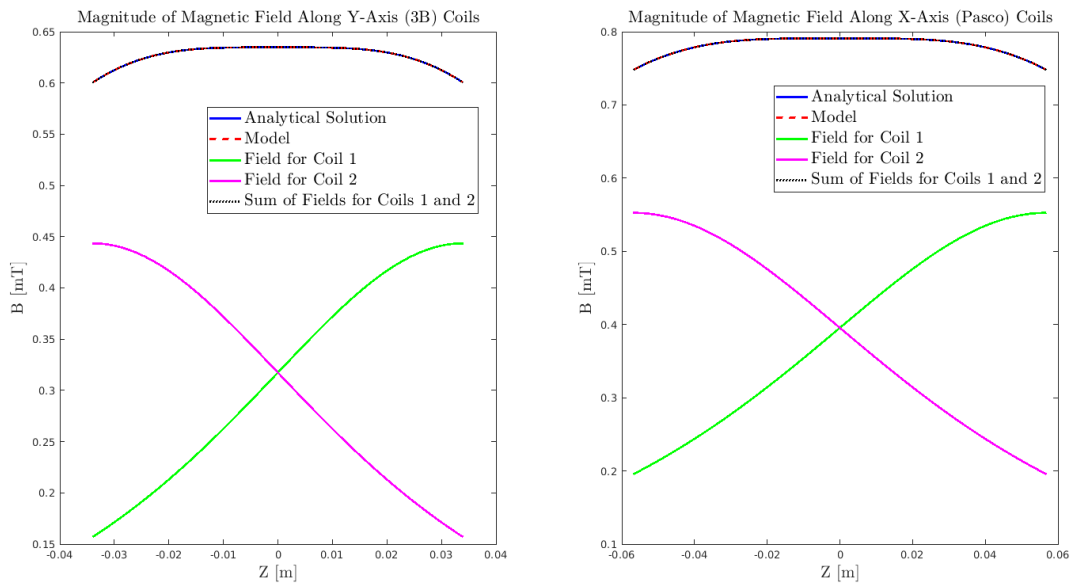

Figure S2: Plots of model predictions for magnetic fields for Pasco coils (along x-axis) and 3B coils (along y-axis). Each plot shows the model prediction (dashed red line), as well as the Biot-Savart Law's predicted fields for each coil individually (green and magenta) and the sum of those fields (in black), as well as the Biot-Savart Law's predicted field for both coils together (solved directly, blue line).
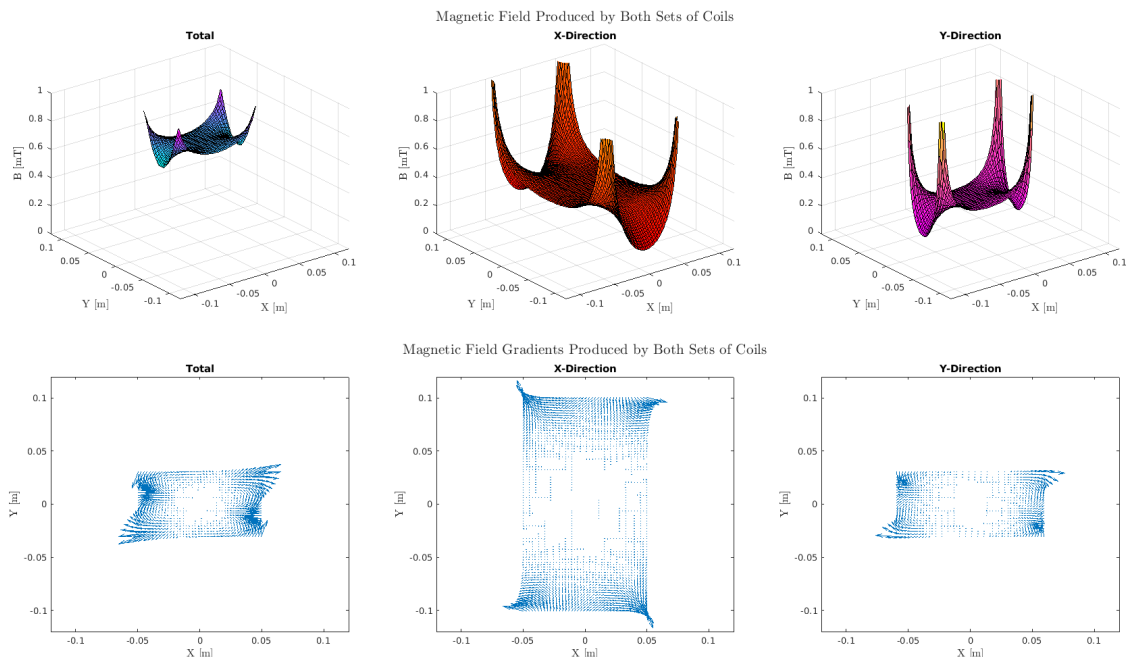
Figure S3: Plots of model predictions for magnetic fields (top) and gradients (bottom) for both Pasco coils (along x-axis) and 3B coils (along y-axis). The left plot shows the sum of the two fields and the next two plots show the fields contributed by each pair of coils individually.

3.2 Magnetic Field Gradient

The magnetic field in our system is represented as a vector comprised of components in the ρ and z directions, that is:

$$\mathbf{B} = (B_\rho \hat{\rho} + B_z \hat{\mathbf{z}})$$

So when we take the derivative of the magnetic field, we must compute the Jacobian as follows:

$$\nabla \mathbf{B} = \begin{bmatrix} \frac{\partial B_\rho}{\partial \rho} & \frac{\partial B_\rho}{\partial z} \\ \frac{\partial B_z}{\partial \rho} & \frac{\partial B_z}{\partial z} \end{bmatrix}$$

$$\nabla \mathbf{B} = (\nabla \mathbf{B}_\rho, \nabla \mathbf{B}_z) = \left((\frac{\partial B_\rho}{\partial \rho} + \frac{\partial B_z}{\partial \rho}), (\frac{\partial B_\rho}{\partial z} + \frac{\partial B_z}{\partial z}) \right)$$

We sum up the columns of the Jacobian to obtain the total contribution of the magnetic field components to the gradient along each direction, and use these terms to write a new vector for the gradient of the magnetic field at every point in the workspace. Using this expression, we can plot the magnetic field gradient as a quiver plot for each set of coils individually and for both of them combined as shown in Figure S3.

In order to properly account for the fact that the B_y component of the field is varying sinusoidally with time, we compute the magnetic field gradient at the swimmer's starting position for one cycle and feed this into our dynamics function (which is in turn passed to the ODE15 solver in MATLAB). The dynamics function interpolates the value of the magnetic field gradient for the current time point and uses that value in the dynamics calculations.

4 Effect of Varying Beta on Swimmer Behavior

We experimented with using different values of β while controlling our nominal cylindrical swimmers. We found that the results were unexpected. We include them here to inspire future investigations into our observations.

First, we found that the milliswimmers demonstrated faster velocities for higher values of the magnetic field amplitude ratio, β. We tested the effect of this parameter by performing frequency sweeps at varying values of β,

using the same three nominal swimmers built with cylindrical links as presented in the main paper. We swept through $f = [1,10]$Hz and $\beta = \{1.0, 2.0, 3.0\}$ experimentally as shown in Figure S4.

Figure S4 shows that there is a moderate increase in the experimentally observed net velocity with increasing β on a per-swimmer basis, specifically for swimmers 1 and 2. However, while swimmer 3's behavior for $\beta = \{1.0, 2.0\}$ in the case of B_x^+ also follows this trend, when β increases to 3.0, swimmer 3 starts to behave differently than swimmers 1 and 2. From $f = [5,9]$Hz, swimmer 3 moves to the right instead of to the left. As swimmer 3 has the largest measured magnetization, it also likely has the largest additional mass contribution from its embedded magnet. We hypothesize that either the stronger magnetic moment or additional inertia may have led the swimmer to rotate around completely, i.e. about $360°$, for higher values of f and β, and not in an oscillatory fashion as we typically observe for $\beta = 1$. The behavior was repeatable across 5 trials for swimmer 3 but was not observed in swimmers 1 or 2, both of which had smaller measured magnetizations. When we consider the data for B_x^-, we can again see that swimmer 3 shows different trends to swimmers 1 and 2. Specifically, for $\beta = \{2.0, 3.0\}$, swimmer 3 shows a slowly increasing (or slightly decreasing) net velocity for the middle of the frequency range before increasing sharply near 10Hz. Conversely, swimmers 1 and 2 show progressively higher net velocities as β increases.

We do not show model predictions in Figure S4 because the model significantly disagreed with the experimental results for higher values of β. In particular, we found that the model overestimated the swimmer net velocity for $\beta = \{2, 3\}$ by an order of magnitude. This may be due to the fact that the swimmer has faster instantaneous velocities at higher values of β, leading to even higher Reynolds numbers that are less well represented by our second order model with modified Stokes drag. The Reynolds numbers for the swimmer actuated by a field with $\beta = 3$ approximately double when compared to those for $\beta = 1$.
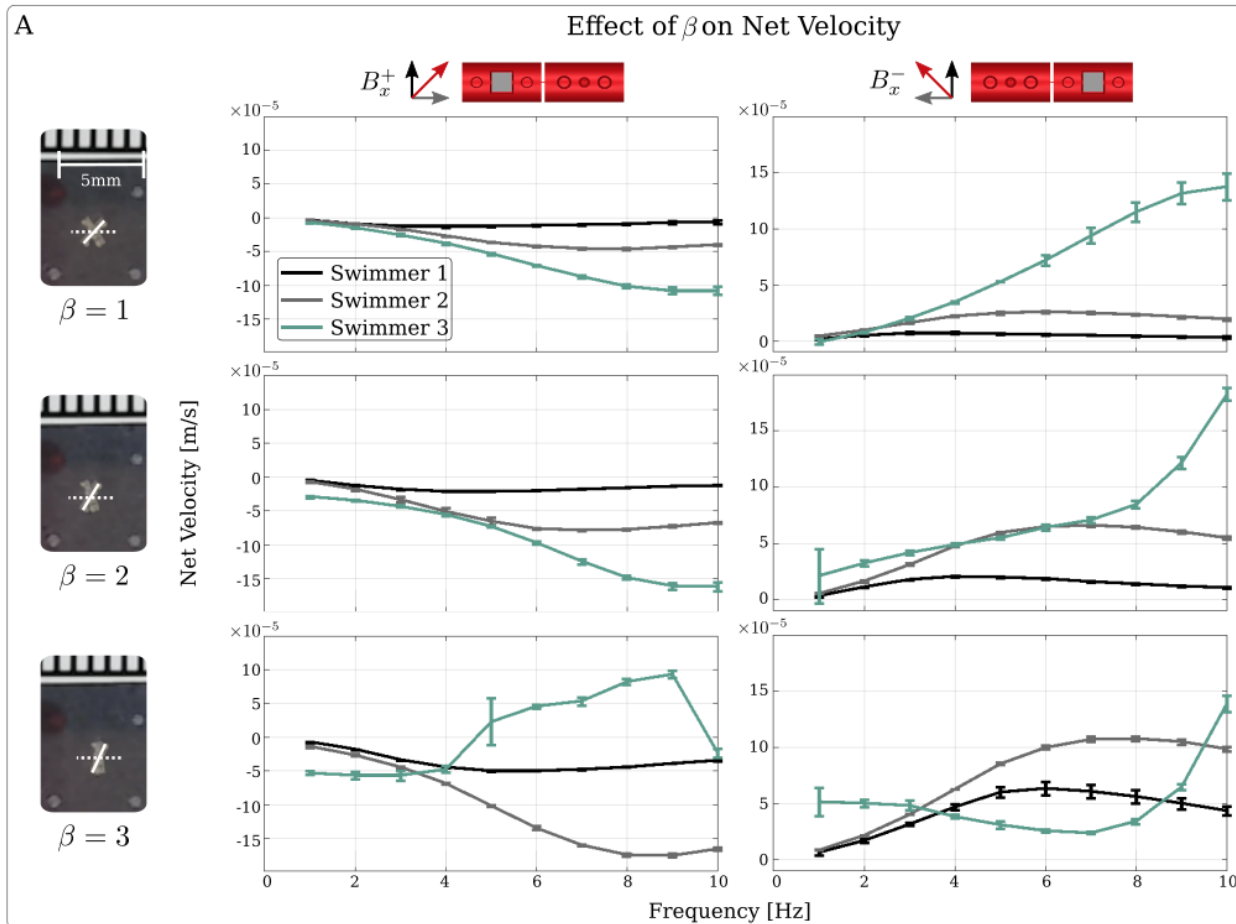
Figure S4: Increasing β generally showed higher net velocities, except for swimmer 3, which showed interesting and unique behavior. We show the observed net velocities for our three nominal, cylindrical swimmers for increasing values of β, from 1 to 3. The images in the leftmost column show the maximum angle that the swimmer sweeps through for each value of β - larger values of β lead to larger sweep angles. The two columns of plots show the mean velocities observed for each of the three swimmers, measured over 5 trials per test. We performed the frequency sweep for both the B_x^+ and B_x^- cases. We found that generally larger values of β led to larger net velocities for swimmers 1 and 2, while swimmer 3 showed a reversal in swimming direction for larger values of β.

# 5 Design of Buoyant Milliswimmers

5.1 Calculations for Air Chamber Sizing

Our buoyant milliswimmers are designed to match the idealized version of our two-link swimmers with both cylindrical and spherical links as closely as possible. The experimental realization uses hollow chambers to trap air to make the swimmer buoyant, which are precisely sized as we explain below. The swimmers are manufactured using two photon polymerization as we describe in Section 9. In this section, we present the calculations used to size the hollow chambers, as well as our reasoning that the drainage ports on the hollow chambers are small enough to prevent the air from escaping while the swimmer is submerged. In Figure S6 we show composite images taken under microscope of each of the three nominal cylindrical swimmers. Note that the images are assembled to show the entire swimmer - each composite image is comprised of two individual images of each link that have been joined and lined up manually to approximate the structure's complete appearance.
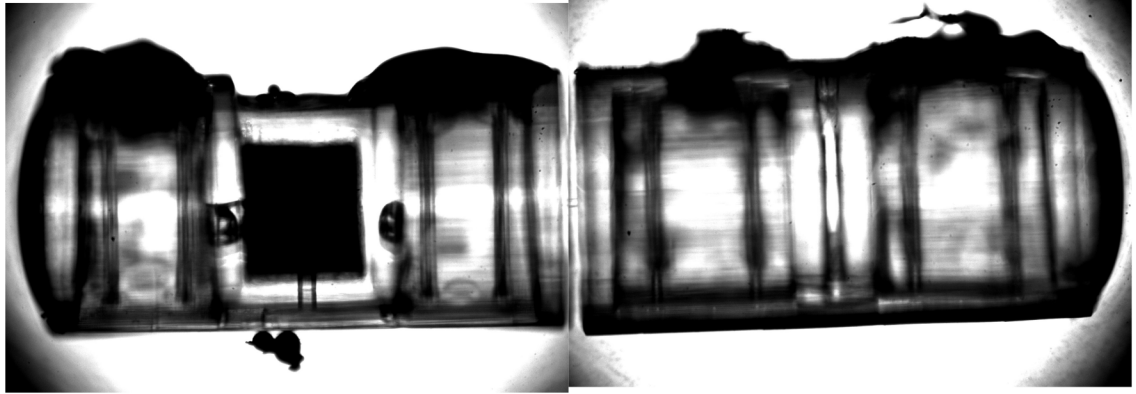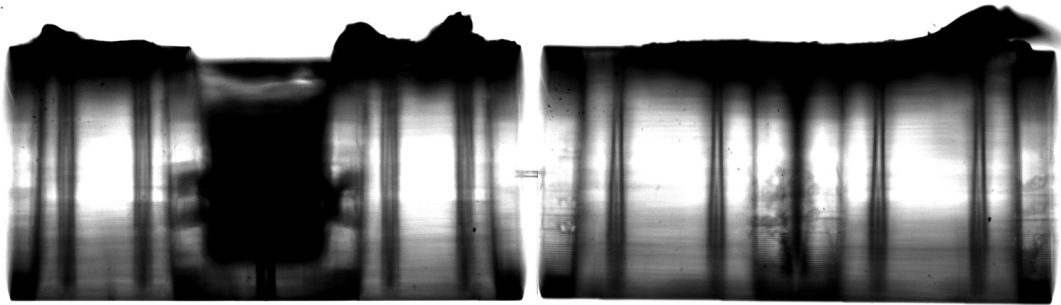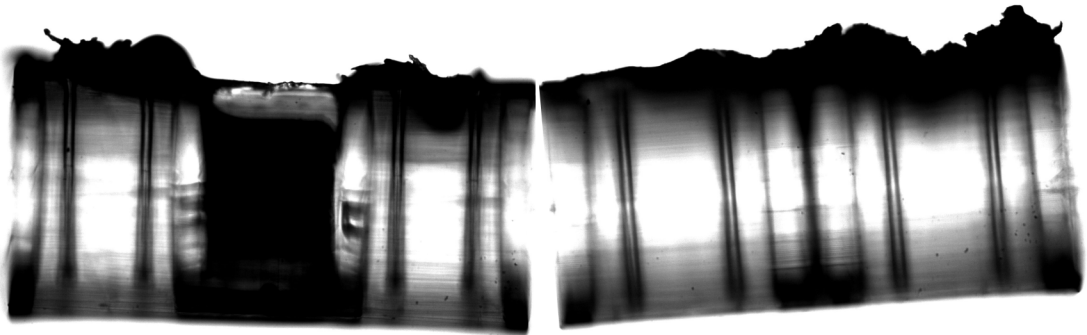
Figure S5: Composite images of three nominal cylindrical milliswimmers. Composite images of each of the three nominal cylindrical milliswimmers. Each composite image is comprised of two individual images of each link that have been joined and lined up manually to approximate the structure's complete appearance.

Our design goal is to build swimmers that are guaranteed to be buoyant even with variations in the added mass of the magnet or in the amount of applied nail polish and glue. This means that the buoyant force, F_b, must be equal to or greater than the weight of the swimmer, F_g:

$$F_b \geq F_g$$

We consider each link individually because they will have different weights according to whether or not they contain the magnet. The buoyant force F_b can be written as:

$$F_b = \rho_{Percoll} \cdot V_{body} \cdot g$$

Here the density of Percoll, the fluid we use in our experiments, is $\rho_{Percoll}$ and the volume of Percoll displaced by the swimmer is V_{body}. Note that the volume of the body varies between links: the magnetic link will have a slightly smaller

displacement volume because there it includes a pocket for holding the magnet. Even with the magnet inserted, the top of this pocket will be open and so we use different values of V_{body} for each link.

We can calculate the weight for each link as the sum of contributing mass elements as follows:

$$F_{\text{g, magnetic link}} = \text{mass of link} + \text{mass of magnet} + \text{mass of residual photoresist} + \text{mass of glue} + \text{mass of nail polish}$$

$$= \rho_{\text{IP-S}} \cdot V_{\text{IP-s}} \cdot g + m_{\text{magnet}} \cdot g + m_{\text{residual}} \cdot g + \rho_{\text{glue}} \cdot V_{\text{glue}} \cdot g + \rho_{\text{nail polish}} \cdot V_{\text{nail polish}} \cdot g \qquad \text{(S22)}$$

$$F_{\text{g, non-magnetic link}} = \text{mass of link} + \text{mass of residual photoresist} + \text{mass of nail polish}$$

$$= \rho_{\text{IP-S}} \cdot V_{\text{IP-s}} \cdot g + m_{\text{residual}} \cdot g + \rho_{\text{nail polish}} \cdot V_{\text{nail polish}} \cdot g \qquad \text{(S23)}$$

Note that the links are made of cured photoresist, specifically IP-S (Nanoscribe). The term for the mass of residual photoresist assumes that we may not be able to fully remove all of the liquid photoresist from inside the hollow chambers during the post-processing steps. We add glue to fix the magnet in place and nail polish to both links to seal the hollow chambers and to increase the visibility of the swimmer during testing.

Link	Nominal, Cyl.	Large L/D, Cyl.	Nominal, Sph.	Dissimilar, Sph.
Magnetic	$0.1902 \times 10^{-9} m^3$	$0.3974 \times 10^{-9} m^3$	$0.5176 \times 10^{-9} m^3$	0.5176×10^{-9}
Non-Magnetic	$0.2046 \times 10^{-9} m^3$	$0.4092 \times 10^{-9} m^3$	$0.5480 \times 10^{-9} m^3$	0.2312×10^{-9}

Table S18: Displacement volumes for each milliswimmer design. This is the volume of Percoll that we estimate is displaced by each milliswimmer link. The magnetic link is also considered as link 1 in our models.

Link	Nominal, Cyl.	Large L/D, Cyl.	Nominal, Sph.	Dissimilar, Sph.
Magnetic (Theoretical)	$0.0862 \times 10^{-9} m^3$	$0.2321 \times 10^{-9} m^3$	$0.3157 \times 10^{-9} m^3$	$0.3157 \times 10^{-9} m^3$
Magnetic (Actual)	$0.0957 \times 10^{-9} m^3$	$0.2327 \times 10^{-9} m^3$	$0.3157 \times 10^{-9} m^3$	$0.3158 \times 10^{-9} m^3$
Error	11.0%	0.3%	0.0%	0.0%
Non-Magnetic (Theoretical)	$0.1237 \times 10^{-9} m^3$	$0.2670 \times 10^{-9} m^3$	$0.3646 \times 10^{-9} m^3$	$0.1311 \times 10^{-9} m^3$
Non-Magnetic (Actual)	$0.1220 \times 10^{-9} m^3$	$0.2678 \times 10^{-9} m^3$	$0.3637 \times 10^{-9} m^3$	$0.1314 \times 10^{-9} m^3$
Error	1.3%	0.3%	0.2%	0.0%

Table S19: Hollow volumes for each milliswimmer design. The theoretical values are the design targets that we calculated using Equations S22 and S23. The actual values are the volumes measured in CAD for each swimmer design. The error is the percentage error between the CAD model and the design target.

Link	SF = 1.1	SF = 1.0	SF = 0.9
Magnetic (Theoretical)	$0.1188 \times 10^{-9} m^3$	$0.1364 \times 10^{-9} m^3$	$0.1579 \times 10^{-9} m^3$
Magnetic (Actual)	$0.1188 \times 10^{-9} m^3$	$0.1362 \times 10^{-9} m^3$	$0.1579 \times 10^{-9} m^3$
Error	0.0%	0.1%	0.0%
Non-Magnetic (Theoretical)	$0.1448 \times 10^{-9} m^3$	$0.1624 \times 10^{-9} m^3$	$0.1839 \times 10^{-9} m^3$
Non-Magnetic (Actual)	$0.1448 \times 10^{-9} m^3$	$0.1625 \times 10^{-9} m^3$	$0.1837 \times 10^{-9} m^3$
Error	0.0%	0.1%	0.1%

Table S20: Hollow volumes for each milliswimmer design investigated during the buoyancy test. The theoretical values are the design targets that we calculated using Equations S22 and S23. The actual values are the volumes measured in CAD for each swimmer design. The error is the percentage error between the CAD model and the design target.

We can use these volumes to compute the buoyant force exerted on each link by Percoll (density of $1300 kg/m^3$),

for example for the magnetic link for the nominal, cylindrical design:

$$F_b = \rho V g$$
$$= (1300 kg/m^3)(0.1902 \times 10^{-9} m^3)(9.8 N/kg)$$
$$= 2.423148 \times 10^{-6} N$$

And for the non-magnetic link:

$$F_b = (1300 kg/m^3)(0.2046 \times 10^{-9} m^3)(9.8 N/kg)$$
$$= 2.606604 \times 10^{-6} N$$

5.2 Sizing of Drainage Ports

We must determine the best diameter of the orifices in the hollow swimmer design to trap a bubble of air when the swimmer is submerged in water. We assume that the air bubble will be trapped in the swimmer while the force applied due to surface tension exceeds the force due to the air's buoyancy. That is:

$$F_{\text{surface tension}} > F_{\text{buoyancy}}$$

We can calculate each of these forces as follows.

5.2.1 Force due to Surface Tension

We know that, according to the Young-Laplace Equation, the surface tension is related to the pressure differential across the bubble's surface as [9]:

$$\Delta P = \frac{2}{R}\sigma$$

Where $\Delta P = p_{\text{inside}} - p_{\text{outside}}$ (i.e. the pressure differential) and R is the diameter of the bubble, and σ is the surface tension. From this, we can compute the force acting on the bubble's entire surface as:

$$F_{\text{surface tension}} = \Delta P \cdot A$$

Where A is the area of the bubble. We assume that the bubble is a sphere of volume equivalent to the air trapped in the links. The volume is approximately $8.2 \times 10^{-11} m^3$, so the radius of the spherical equivalent is $R = 2.695 \times 10^{-4}$m $= 269.5\mu$m. (Recall $A = 4\pi R^2$.) We obtain a pressure differential of 534N/m^2, and a surface tension force of 4.87×10^{-4}N.

5.2.2 Force due to Buoyancy

We can also compute the force due to buoyancy as follows [9]:

$$F_{\text{buoyancy}} = \rho_{\text{water}} \cdot V \cdot g$$

Where ρ_{water} is the density of water (997 kg/m3) and g is gravitational acceleration. V is the volume of the bubble. We calculate a buoyant force of 8.01×10^{-7}N.

This result shows that the buoyant force is three orders of magnitude smaller than the surface tension force acting on the bubble. This means that it is unlikely for the current design to allow air to escape.

5.2.3 Bubble Size When Surface Tension is Equal to Buoyant Force

Another way to check that our drainage ports are small enough is to calculate how large the air bubble would need to be to balance the buoyant force and the surface tension force. We can calculate it as follows:

$$F_{\text{buoyancy}} = F_{\text{surface tension}}$$
$$\rho_{\text{water}} \cdot V \cdot g = \Delta P \cdot A$$
$$\rho_{\text{water}}(\frac{4}{3}\pi R^3)g = \frac{2}{R}\sigma(4\pi R^2)$$
$$R^2 = \frac{8\sigma\pi}{\rho_{\text{water}}\pi g \frac{3}{4}}$$
$$R = \sqrt{\frac{10.67\sigma}{\rho_{\text{water}}g}}$$

The bubble radius in this case is 8.87×10^{-4}m. This value is approximately 3 times larger than the bubble size we have in our air chamber, indicating that the volume of air we have trapped is too small to have enough buoyancy to escape the hollow chamber.

5.2.4 Bubble Size Emerging from Our Drainage Port Size

We can also check our design by asking what bubble size would emerge from an orifice that is the same size as our milliswimmer design. We can compute this as [9]:

$$d_p = \left(\frac{6d_o\sigma}{\Delta\rho g}\right)^{1/3}$$

Where d_p is the diameter of the bubble, d_o is the diameter of the orifice. Using this calculation, we estimate the bubble will have a radius of 787um. This is bigger than the actual orifice so that suggests that the pressure exerted by the trapped air will need to be significant in order to push the bubble out. In fact, the pressure differential will need to be:

$$\Delta P = \frac{2}{R}\sigma$$

In this case we estimate the pressure differential will be 2880 N/m^2. But this is about 5 times the pressure that we estimate is in the bubble of air trapped in the milliswimmer (183N/m^2), so it is unlikely for a bubble to escape from an orifice of size 100μm unless we significantly increase the pressure in the bubble.

5.2.5 Summary of Air Bubble Calculations

We have learned the following:

1. The buoyant force exerted by our air bubble is 1000 times smaller than the surface tension force exerted on the bubble's surface. It is therefore unlikely that the bubble will exit the hollow chamber in the milliswimmer because the surface tension dominates.

2. If the buoyant force were to match the surface tension force, we would see bubbles with a radius of 0.89mm. This is a much larger size than the milliswimmer's orifices so it is unlikely that we will see the bubble escape.

3. If we were to release a bubble from an orifice with the size matching the milliswimmer design, then it would have a radius of 787um. This indicates that the bubble would expand upon being released from the chamber, thereby indicating that it would need to contain a significantly high internal pressure.

4. The pressure differential at the orifice would have to be about 5 times larger than the balanced case - that is, it would be about 2880 N/m^2. The expanded bubble (see item 3) would have a pressure differential closer to the balanced case (see item 2) of 183 N/m^2.

In total, the current orifice sizes are likely sufficient to trap air in the swimmer's hollow chambers.

5.3 Measurement Data for Three Nominal Cylindrical Swimmers

This section includes the measurement data summarized in Table 1 in the main text, as well as the images used to obtain these measurements. Note that, across the three images, the minimum measurement resolution was 1μm. We report additional decimal places here using the raw measurement data obtained from measurements taken in FIJI for completeness of calculation; values are rounded to the nearest μm in Table 1 in the main paper [10].

Table S21: Raw measurement data for swimmer 1. Minimum resolution across the three swimmers 1μm, additional decimal places are reported here using the raw measurement data obtained from measurements taken in FIJI for completeness of calculation.

	Link 1 Length [μm]	Link 1 Diameter [μm]	Link 2 Length [μm]	Link 2 Diameter [μm]
1	1014.337	502.805	976.663	494.773
2	1022.771	494.494	976.521	506.977
3	1022.307	498.805	993.282	494.494
4	1014.133	486.201	993.456	494.564
5	1031.078	490.497	980.994	502.805

Table S22: Raw measurement data for swimmer 2. Minimum resolution across the three swimmers 1μm, additional decimal places are reported here using the raw measurement data obtained from measurements taken in FIJI for completeness of calculation.

	Link 1 Length [μm]	Link 1 Diameter [μm]	Link 2 Length [μm]	Link 2 Diameter [μm]
1	988.995	497.529	994.325	492.03
2	1005.015	497.002	1002.751	499.61
3	1002.929	492.463	997.428	503.233
4	997.614	497.736	984.06	490.212
5	997.614	500.704	994.325	497.529

Table S23: Raw measurement data for swimmer 3. Minimum resolution across the three swimmers 1μm, additional decimal places are reported here using the raw measurement data obtained from measurements taken in FIJI for completeness of calculation.
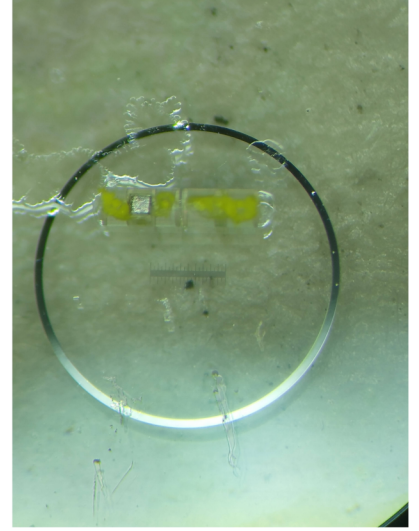
	Link 1 Length [μm]	Link 1 Diameter [μm]	Link 2 Length [μm]	Link 2 Diameter [μm]
1	1022.609	515.942	961.934	506.697
2	1028.583	509.813	971.22	503.7
3	1010.524	500.776	998.298	503.672
4	1013.435	516.023	1004.366	518.914
5	1007.441	506.697	1031.76	515.835
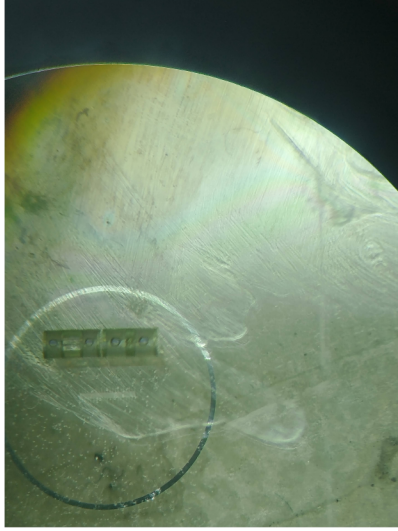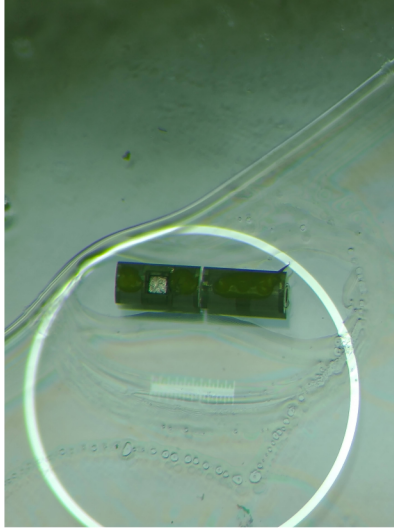
| Swimmer 1 | Swimmer 2 | Swimmer 3 |

Figure S6: Brightfield microscopy images of three nominal cylindrical milliswimmers. Images of each of the three nominal swimmers taken using brightfield microscopy. Scale bar (1mm) included in each image.

6 Magnetic Properties of Ferromagnetic Cube

We source the magnets for our milliswimmers from SuperMagnetMan. They are cubes that are 0.25mm long on each side, and made of neodymium 50. Our model requires information about the magnetic moment of these magnets, expressed as a product of the volume (V) and the magnetization per unit volume ($\mathbf{M}$):

$$\xi = V\mathbf{M}$$

The manufacturer provides data on the magnetic moment, which we can use to to find $\mathbf{M}$ by dividing ξ by the volume of the link. Note that the magnetization per unit volume is a vector, $\mathbf{M} = M(h_{i,t}\hat{t}_i + h_{i,n}\hat{n}_i)$, where M is the scalar magnitude of the magnetization per unit volume vector, $\mathbf{M}$. We assume that the magnetic moment calculated from the manufacturer's data is equivalent to the magnetic moment along the transverse axis of the milliswimmer, i.e. along the $\hat{t}_i$ direction.

We use the manufacturer's reported remanence, B_r, to compute the magnetic moment of these ferromagnetic cubes, ξ, as follows:

$$\xi = \frac{1}{\mu_0}B_r V$$

We need to compute M, which can be found as above by computing $M = \frac{\xi}{V}$. Therefore:

$$
\begin{aligned}
M &= \frac{\frac{1}{\mu_0}B_r V}{V} \\
&= \frac{1}{\mu_0}B_r \\
&= \frac{1}{4\pi \times 10^{-7}H/m}(1.39T) \\
&= 1.11 \times 10^6 \frac{A}{m}
\end{aligned}
$$

Just to confirm the units are correct we can write the units from the expression above as follows:

$$M = \frac{1}{\left[\frac{kg \cdot m^2}{s^2 \cdot A^2}\right]\left[\frac{1}{m}\right]} \cdot \left[\frac{kg}{A \cdot s^2}\right] = \frac{A}{m}$$

While corresponding with the manufacturers, they noted that their reported value of the magnetic moment of the ferromagnetic cubes is an ideal value, which does not account for some details in the manufacturing process. For example, the cubes have a coating which reduces the total volume of neodymium present in the product. Moreover, there may be small surface blemishes on the cubes due to the manufacturing process, which could further reduce the overall volume of magnetic material in the magnet. We continue to use the ideal value of the magnetization of the magnet for our modeling, but it should be noted that this may be an overestimate of the true value.

If we assume that the magnets are the nominal size then we can compute the magnetic moment, m, as:

$$m = MV$$
$$= (1.11 \times 10^6 \frac{A}{m})(250 \times 10^{-6}m)^3$$
$$= 1.73 \times 10^{-5} Am^2$$

We can convert the units from Am^2 to emu given that $1emu = 10^{-3}Am^2$ therefore:

$$m = (1.73 \times 10^{-5}Am^2) \cdot \frac{1emu}{10^{-3}Am^2}$$
$$= 0.0017emu$$

As we can see in the subsequent section on the data obtained from the vibrating sample magnetometer, this value turned out to be an underestimate of the magnetic moment of the magnets used in these experiments.

7   Helmholtz Coil and Motor Controller Time Constants

We test our milliswimmers in sinusoidally-varying magnetic fields that oscillate at frequencies up to 10Hz. This limit is driven by the lag in the laptop used to control the current to the coils, but we also verified that the coils' time constants were fast enough that they would not also limit the range of actuating frequencies. We derive those time constants below.

First, we can model each individual Helmholtz coil as a circular coil inductor [11], as follows:

$$L = \mu_0 r N^2 \left[\ln\left(\frac{8r}{a}\right) - 2\right]$$

Where the inductance, L, is a function of the magnetic permeability in a vacuum, μ_0, the radius of the coil, r, the wire diameter a and the number of turns, N.

For the Pasco coils, this results in:

$$L_{Pasco} = (4\pi \times 10^{-7}H/m)(0.105m)(500^2)\left[\ln\left(\frac{8(0.105m)}{(0.00064m)}\right) - 2\right]$$
$$= 0.1709H$$

And for the 3B coils this is:

$$L_{3B} = (4\pi \times 10^{-7}H/m)(0.068m)(320^2)\left[\ln\left(\frac{8(0.068m)}{(0.00064m)}\right) - 2\right]$$
$$= 0.0415H$$

We use a simplifying assumption that there is negligible magnetic or electrical coupling between the coils, and so we can calculate the total inductance for a pair of Helmholtz coils as the sum of two inductors in parallel:

$$\frac{1}{L_{total}} = \frac{1}{L_1} + \frac{1}{L_2}$$

$$L_{total} = \frac{L_1 L_2}{L_1 + L_2}$$

So for the Pasco coils, we find:

$$L_{total,Pasco} = \frac{(0.1709H)^2}{2(0.1709H)}$$

$$= 0.0854H$$

And for the 3B coils we obtain:

$$L_{total,3B} = \frac{(0.0415H)^2}{2(0.0415H)}$$

$$= 0.0208H$$

We can model the circuit for one pair of coils as an RL circuit - that is, as a circuit containing a resistor and an inductor in series with a power supply, where the coils provide both the resistance and the inductance. The total resistance of each pair of coils in parallel can be found similarly to the inductance. The Pasco coils report that they are constructed using 22AWG wire, which has a resistance per unit length of 52.7Ω per 1000m. Therefore the resistance of one coil is:

$$R_{Pasco} = \frac{resistance}{length} \cdot length$$

$$= \frac{resistance}{length} \cdot n_{turns} \cdot 2\pi radius$$

$$= \frac{52.7\Omega}{1000m} \cdot (500)(2\pi)(0.1137m)$$

$$= 18.8\Omega$$

And so the total resistance of the two Pasco coils in parallel is:

$$R_{total,Pasco} = \frac{(18.8\Omega)^2}{2(18.8\Omega)}$$

$$= 9.4\Omega$$

The 3B coils directly report their effective impedance as 6Ω. Now we can compute the time constant for each pair of coils as follows:

$$\tau = \frac{L}{R}$$

$$\tau_{Pasco} = \frac{0.0854H}{9.4\Omega} = 0.009s$$

$$\tau_{3B} = \frac{0.0208H}{6\Omega} = 0.003s$$

Given these time constants, we can see that the maximum frequency we could reasonably operate at would be $f = \frac{1}{T} = 10.009s = 111$Hz for the Pasco coils and 333Hz for the 3B coils. To avoid aliasing, we might choose to operate at the Nyquist frequencies instead, which would reduce our effective maximum sampling frequency by half, to 55.5Hz and 167Hz, respectively. These frequencies are faster than the 10Hz limit that we found our laptop imposed on our setup, so we can conclude that we do not need to make adjustments in our control setup to accommodate for our coils' time constants.

8 Manufacturing Procedure for Milliswimmers

In this section we present the manufacturing process for building our milliswimmers. The manufacturing process begins after the CAD models have been developed as described above. In this section, we first describe the two-photon polymerization (TPP) process for making the base milliswimmer structure, and then we describe the process of adding nail polish for high-contrast visualization of the swimmers and installing the magnet for actuation of the swimmers.

8.1 Two-Photon Polymerization of Milliswimmer Base Structure

As described in the main paper, the milliswimmers are constructed using two-photon polymerization (Nanoscribe Photonic Professional GT2 platform). Glass coverslips coated in indium tin oxide (ITO) on one side are used as the printing substrate (part number DiLL 0000381). The conductive side is spin-coated in a layer of Dextran at 2000 rpm for 1 minute to ensure the print can be easily removed from the coverslip after printing. A dip-in laser lithograph (DiLL) printing process is used with IP-S resin and a 25X objective. Note that we selected IP-S over IP-PDMS for a more robust, rigid swimmer body. We were concerned that the swimmer's side walls made with IP-PDMS might not be able to contain the magnet when placed in the external magnetic field and that the magnet would tear through the wall.

The standard IP-S 25X ITO Solid (3D MF) settings are used as a starting point in the DeScribe application. The most significant changes to the slicing settings are setting the cross-hatching to alternate orthogonal directions on every layer, and to ensure that individual blocks are supported by blocks in the previous layer.

We use the following parameters for creating the print recipe in DeScribe:

1. The CAD model is made in Solidworks at the millimeter scale, and then scaled down to the micrometer scale in DeScribe.

2. We use the 25X objective because the 63X has a limited height range that it can operate over before the higher magnification objective's focal plane exerts limitations on the size of the printed object.

3. We begin with the IP-S 25X ITO solid (3D MF) settings and modified them as follows.

4. We used fixed slicing mode, simplification tolerance = 0.05 and allowed for fixing self-intersections.

5. We set the fill mode to solid.

6. The hatching distance was 0.5, with 0 contour count and base slice count 2.

7. The hatching angles were set to be 90 degrees, 90 degrees to form orthogonal, alternating cross-hatching across layers.

8. Block sizes were typically 200 to 300 micrometers long.

9. We manually manipulated the size and location of the blocks to ensure that the base of each block was always resting on material from a previous layer. In particular, we ensured that every block on the base layer was connected to the flat pad that is in contact with the glass substrate so that the entire print stuck to the glass.

10. We reviewed the printing process in DeScribe's simulation tool to be sure that each block was connected to material on previous layers.

11. The print output z-direction is set to "upwards" because dip-in inverts the print (the substrate is the highest point and we print "down" towards the top of the print itself).

After printing is complete, the result is developed in propylene glycol monomethyl ether acetate (PGMEA) for 45 minutes and then washed in 99% isopropyl alcohol for 3 minutes.

8.2 Manual Assembly of Complete Milliswimmer

As described in the main paper, after printing and developing, we first add opaque nail polish to each link to ensure that we can visualize the swimmer with our camera during testing. The nail polish is also used to seal the drainage ports as a second method for ensuring that the air trapped in the hollow chambers does not escape. We apply the nail polish using a small sewing needle while observing the process under a microscope at 2 to 4X magnification. Note that this step must be completed before adding the magnet because our sewing needle is also magnetic and we want to avoid inadvertently damaging the swimmer via a magnetic pull between the magnet and the needle.

Next, the ferromagnet (Supermagnetman C0005-10) is placed by hand in the appropriate pocket in the design using forceps. We always pick up 3 magnets connected together and orient them parallel to the longitudinal axis of the swimmer before pushing the first magnet into the pocket of the swimmer body. Note that because we always use the stack of 3 magnets to keep track of the magnets' magnetization direction, we can always ensure that the milliswimmer's magnetization direction is along its longitudinal axis. (It is still possible for separate milliswimmers to have their north poles oriented 180 degrees apart; this occurred when building the SF = 1.1 swimmer for the buoyancy test.)

After the magnet is added, a small droplet of glue is placed in the magnet pocket with the forceps to ensure that the magnet is fixed in place. Be careful not to add excess glue as this could fix the milliswimmer to the glass substrate and make it impossible to remove the swimmer from the glass substrate (the removal process is described in a subsequent section on experimental setup processes). The assembly is allowed to dry overnight prior to testing.

9 Experimental Process for Milliswimmers

9.1 Overview

We place the milliswimmers in a uniform magnetic field created by two orthogonal pairs of Helmholtz coils. A webcam is used to record the motion of the milliswimmers. We apply sinusoidally-varying magnetic fields to the milliswimmers and record their response using the camera. The resulting video data is analyzed as described in a subsequent section. In the remainder of this section, we describe the set of experiments that we conduct and the experimental procedure.

9.2 Experimental Set Up Procedure

Our experimental set up procedure for the milliswimmer swim tests is as follows:

1. Set up the Helmholtz coils. Ensure that the stage has a dark sheet of paper with white grid markings fixed at the location where the swimmer will be tested. The test position should also have fixture points and/or double sided tape ready to hold the Petri dish containing the milliswimmer in place. The exact test region should be marked using a bright color so that it is easy to repeatedly place the milliswimmer in the same position for all tests.

2. Prepare the Petri dish containing the milliswimmer. First clean the surfaces of the dish thoroughly with 70% isopropyl alcohol and a Kimwipe to ensure visibility all the way through the dish during testing.

3. Place the glass coverslip with the milliswimmer attached to it in the center of the Petri dish.

4. Using a clean plastic dropper, slowly add Percoll to the Petri dish, being careful not to disturb or damage the milliswimmer. As Percoll is being added to the dish, the Dextran coating on the glass coverslip will start to dissolve in the Percoll and the milliswimmer will come free, rising to the surface of the fluid. If this does not happen, use the plastic dropper to create a bubble and use the bubble to push against the milliswimmer. It has been found experimentally that minor disturbances are sufficient to free the swimmer from the Dextran. Use caution when applying large forces as it is easy to break the joint between the two links. In a 35mm diameter, 10mm deep Petri dish, the height of the Percoll should be approximately 5-8mm and the milliswimmer should be floating at the top of the fluid.

5. Use a small magnet (we have attached a small refrigerator magnet to a T-handle Allen key for ease of use) to pull the milliswimmer to one side of the dish, away from the glass coverslip. Remove the glass coverslip with forceps and clean it off with water, disposing of the Percoll per relevant safety guidelines. Retain the glass coverslip for the end of the experiment because the milliswimmer can be stored on the same coverslip between experiments, as long as the coverslip is clean. (More details on preparing the milliswimmers for storage is provided below.)

6. Use the plastic dropper to pop any bubbles that may have been created when the glass coverslip was removed from the Petri dish. In particular, remove any small bubbles on the bottom surface of the dish because these can interfere with the tracking software during the data analysis procedure. Be sure not to damage the milliswimmer during this process (the magnet can be used to keep the milliswimmer to one side of the dish).

7. Ensure the Percoll has come to room temperature and that any residual condensation on the Petri dish has been removed with a Kimwipe. It is important to ensure that there is full visibility through both the lid and the base of the dish.

8. Examine the Percoll in the Petri dish, specifically looking for any particulates or "aggregated" Percoll that may have dried and formed a small, solid "chip" floating on the fluid surface or attached to the sides of the dish. These "chips" can attach to the milliswimmer, affecting its motion, so we want to ensure that these chips have been removed from the test environment before starting. Any chips can be removed from the fluid using a Kimwipe or forceps. We also recommend replacing the used Percoll with fresh Percoll approximately once per 10 experiments.

9. We also recommend briefly examining the milliswimmer while it is floating in the open container of Percoll under a microscope (low magnification, i.e. 2X to 10X, is sufficient). We do this to check if any particulate has attached to the milliswimmer itself. If particulate is identified on the body of the milliswimmer, we first aspirate the Percoll using a clean plastic dropper and transfer the Percoll to a storage container. Then we wash the milliswimmer 3-5 times with deionized water using a second clean plastic dropper, before checking if the particulate has been removed via the microscope. If the particulate has been removed, we replace the Percoll in the dish and proceed to the next step. Otherwise, we continue to wash the milliswimmer with deionized water until the particulate has been removed. As a last resort, it is possible to remove the particulate with forceps, but we do not recommend this because it increases the risk of damaging the milliswimmer.

10. Once any particulate has been removed from the test environment and the milliswimmer, place the lid on the Petri dish and use lab tape to seal the container. It is important to thoroughly seal the container to prevent the water solvent in the Percoll from evaporating and changing the viscosity of the fluid during testing.

11. Use double-sided tape to attach a small ruler to the lid of the Petri dish. Make sure the ruler is at one edge of the dish so that the milliswimmer (which will be in the middle of the dish during testing) is not obstructed. The ruler can be used to establish the scale of the videos during the data analysis procedure.

12. Place the sealed Petri dish on the stage in the middle of the Helmholtz coils. The dish should be held in place against fixture points using double-sided tape. The test region as marked on the paper on the stage should be located underneath the approximate middle of the Petri dish.

13. Use the magnet to pull the milliswimmer to the desired test region.

9.3   Milliswimmer Testing Procedure

The experimental setup is now complete and testing can begin. These tests include 3 control tests and 10 swim tests at different actuation frequencies. We conduct one set of tests (i.e. one set of control and swim tests) before repeating the set, and we do this 5 times. This ensures that the control tests capture any variation in the experimental setup that may occur during the experiment. (Overall it takes approximately 1.5 - 2 hours to perform the n = 5 repetitions of the test set including control and swim tests for one milliswimmer.)

The control tests include first a test to record the motion of the swimmer in the absence of any externally applied magnetic field (the "drift" test). The second control test applies the maximum magnitude of the magnetic field in the horizontal direction **only** to capture any effects of the magnetic field gradient in that direction during the application of sinusoidally varying magnetic fields (the "bx" test). The third test applies the sum of the maximum magnitude in the horizontal **and** vertical directions (the "bxby" test). Note that the magnitude of the horizontal and vertical components should match the maximum values of these components for a sinusoidally varying magnetic field with the appropriate β value for the experiment currently being conducted.

The test procedure is described below:

1. Ensure the milliswimmer is placed in the center of the test region. The magnet (which we have attached to a T-handle Allen key) can be used to pull the swimmer to the desired location through the sealed Petri dish. When not in use, be sure to store the magnet far from the Helmholtz coil setup to avoid interfering with testing.

2. Turn on the webcam and record the milliswimmer's motion for 1 minute in the absence of any externally applied magnetic field (the "drift" test). When the recording is finished, label the file appropriately before moving on to the next test (this avoids any confusion in the video files as the testing continues).

3. If the milliswimmer has drifted, use the magnet to return it to its original position.

4. Configure the coils to generate the maximum field in the horizontal direction (the "bx" test as described above). Turn on the webcam to begin recording, and then turn on the magnetic field once the recording has started. Record video for one minute, then save and label the file. Ensure the field has turned off.

5. If the milliswimmer has drifted, use the magnet to return it to its original position.

6. Configure the coils to generate the maximum field in the horizontal and vertical directions (the "bxby" test). Turn on the webcam to begin recording and then turn on the magnetic field. Record the video for one minute, then save and label the file. Ensure the field has turned off.

7. If the milliswimmer has drifted, use the magnet to return it to its original position.

8. Configure the coils to generate a sinusoidally varying magnetic field with the appropriate β value at a frequency of 1Hz. Turn on the webcam to begin recording and then turn on the magnetic field. Record the video for one minute, then save and label the file. Ensure the field has turned off. If the milliswimmer has displaced, use the magnet to return it to its original position.

9. Repeat the previous step for increasing values of actuation frequency, that is from 1 to 10Hz in increments of 1Hz.

10. Repeat the entire procedure 4 more times for a total of 5 videos per test case. Save all of the data in an appropriate directory.

9.4   Storing Milliswimmers Procedure

After testing for a particular milliswimmer is complete, we remove the milliswimmer from the Petri dish, and the Percoll, and store them for later use. (Note that if you want to store the Petri dish with the current milliswimmer, for example between experiments, we typically store the entire sealed Petri dish in a 4°C refrigerator.) The procedure for dismantling the experimental Petri dish is as follows:

1. Once the requisite experiments for the milliswimmer is complete, remove the Petri dish from the Helmholtz coil setup.

2. Remove the lab tape from the Petri dish. We recommend only reusing the tape 1-2 times before replacing it to ensure the tape always maintains a good seal.

3. Remove the lid from the Petri dish.

4. Use the magnet to pull the milliswimmer to one side of the dish. Use a set of forceps to place the glass coverslip for the milliswimmer at the bottom of the dish, submerged in Percoll. Be careful not to damage the milliswimmer while inserting the coverslip.

5. Use the magnet to pull the milliswimmer to float directly above the coverslip.

6. Using a clean plastic dropper, aspirate the Percoll from the Petri dish. We typically store and reuse the Percoll for several days of testing. (The Percoll is stored at 4°C per the manufacturer's instructions.) As discussed in the set up instructions, be sure to regularly replace the Percoll to avoid the formation of "chips" that can attach to the milliswimmer and alter its motion.

7. As the Percoll is aspirated out of the dish, the milliswimmer should settle onto the glass coverslip underneath it. Once the Percoll has been removed, use forceps to carefully pick up the coverslip from the Petri dish and place it in a separate container (we use a small box with a snap lid designed to accommodate glass coverslips). The Percoll can be stored in a sealed container in a refrigerator at 4°C.

8. Before closing the milliswimmer storage container, use a clean plastic dropper to wash the milliswimmer with deionized water 3-5 times. Inspect the milliswimmer after washing under the microscope to ensure that all the Percoll has been removed (Percoll has a different refractive index and appearance than water). It is important to thoroughly remove all traces of Percoll from the milliswimmer after use, because any remaining Percoll will dry onto the milliswimmer, changing its outer profile and affecting future swim tests with that swimmer. We have found experimentally that it is difficult to remove the Percoll once it has dried.

9. Once the milliswimmer is clean and stored in a separate sealed container on its glass coverslip, clean the Petri dish thoroughly with deionized water, disposing of the water per relevant safety regulations.

9.5   Magnetometer Data Collection Procedure

We use a magnetometer to capture the magnetic field data. We do not capture magnetometer data during the actual swim tests described above for several reasons. The first is that placing the magnetometer at the point of interest would obscure the camera's view. Secondly, we found that the magnetometer's integrated chip tended to heat the Percoll, which affected the fluid's properties and added a confounding variable to the swim tests.

Instead, we perform a series of "dry runs" where we record the magnetic field that will be applied to the milliswimmer separately from the actual swim tests that we record with the camera. The magnetic field is not measured while video is being recorded. It is assumed that the field will be the same as what was recorded during the "dry run." We capture magnetometer data for each of the tests performed as described above, including the "drift" case where the magnetic field is turned off. The experimental procedure for recording the magnetometer data is as follows:

1. Place the sensor of the magnetometer at the starting point used in the milliswimmer tests. Note the orientation of the magnetometer sensor so that its internal x, y and z axes can be matched to the experimental setup during data analysis.

2. Open the magnetometer software and record approximately 20 seconds of data for the "drift" case where the magnetic fields are turned off. Our magnetometer records data at approximately 1000Hz so this step gathers approximately 20,000 data points for our analysis. We chose 20 seconds so that we would obtain approximately a minimum of 20 full cycles of the magnetic field in the case where the actuation frequency is 1Hz. Save the file and label it appropriately to avoid confusion.

3. Repeat the previous step 4 more times for a total of 5 readings of the ambient environment at 20 seconds each.

4. Configure the coils to generate the "bx" field, that is, the maximum horizontal component of the magnetic field only. Record approximately 20 seconds of data, then save the file. Turn off the magnetic field.

5. Repeat the previous step 4 more times for a total of 5 readings of the "bx" configuration at 20 seconds each. After each test, turn off the magnetic field, then turn it on again before restarting the recording.

6. Repeat the previous two steps for the "bxby" field configuration, where the maximum of both the horizontal and vertical components are switched on, as well as for all of the test frequencies in the range of [1, 10]Hz.

At the end of this test procedure, we will have a set of 5 readings per test (including both controls and frequency tests). Each reading contains 20 seconds of data, or 20,000 points. We describe the data analysis process for this dataset in Section 10.

9.6   SEM Imaging Procedures

After experimentation with the milliswimmer was complete, SEM images were collected for qualitative assessment of the structure's surface profile. Prior to imaging, milliswimmer were cleaned with water, IPA, and filtered nitrogen. They were gently attached to SEM specimen mounts in the desired orientation using carbon mounting tape. Samples

were sputter coated with a 7nm gold layer using an EMS Q300T D Plus Dual Target Sequential Sputtering System. The milliswimmer were imaged using a Nanoscience Phenom XL Desktop SEM. Samples were imaged with an acceleration of 10 kV and magnifications ranging from 200x to 2800x. They were imaged along their x and z axes as well as in an isotropic view using an angled stub. Milliswimmer were broken at the flexible joint to allow better access for imaging the joint. Representative SEM images of the flexible link, the cylindrical milliswimmer link, and the spherical milliswimmer link are shown in Figure S7.
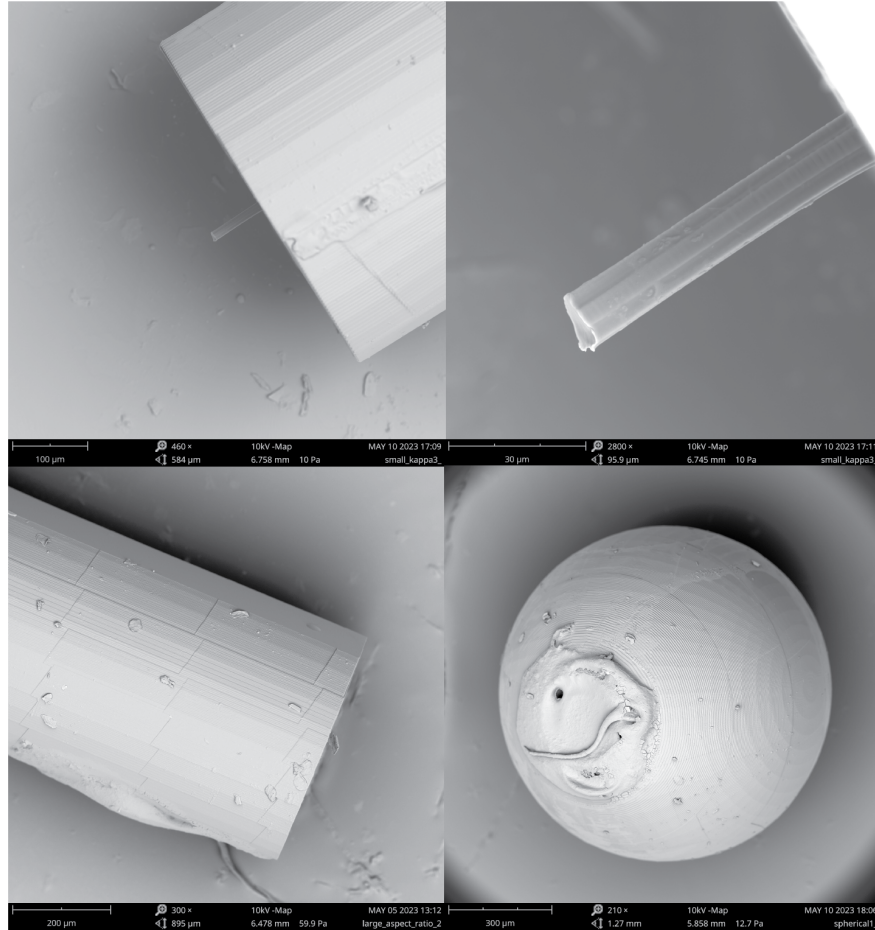

Figure S7: Grayscale SEM images of the flexible joint, cylindrical link, and spherical link of the milliswimmer. Lines and ridges visible on the milliswimmer's surface show the layers created when printing using TPP.

10 Magnetometer Data Analysis

In this section we describe our analysis process for our magnetometer data. We use a 3-axis magnetometer to collect 5 sets of magnetic field readings for each actuation test as described in Section 9. This data is imported to MATLAB for analysis.

First, we analyze the data from the control tests ("drift", "bx" and "bxby"). Specifically, we import the raw data and first smooth it using a moving mean with a sliding window of width 50. We then calculate the mean magnitude of the field in the x, y and z directions for each data sample. (Note that our magnetometer was oriented such that the magnetometer's x, y and z axes match the x, y and z axes of the actual experimental setup.) We then compute a mean magnitude over the 5 samples for each control test, as well as the corresponding standard deviation.

We use the mean Bx and By values from the "bxby" control test to calculate the true β values for each experiment. We noted that the "drift" test data showed that the Bx and By readings were approximately 0.1mT even when there was no command being sent to the power supply. We suspect that this small magnetic field could be due to ambient

magnetic noise or a slight offset in the sensor. We therefore subtracted the mean Bx and By values calculated for the "drift" data from the corresponding values in the "bx" and "bxby" datasets. We calculated the β values from these corrected Bx and By values.

In addition to calculating the true β values from the magnetometer data, we also used it to extract the mean and standard deviation of the oscillation frequency. We did this by applying a Fast Fourier Transform (FFT) to the By signal for each frequency test and then extracting the frequency corresponding to the maximum power reading across the frequency spectrum. We calculated the mean frequency across the 5 data samples, as well as the corresponding standard deviation.

11   Video Data Analysis

We analyze the video data obtained from the milliswimmer swim tests using FIJI [10] to extract the raw trajectory data from the videos, and MATLAB to calculate the velocities and headings of the swimmer trajectories, as well as to plot the findings. All of the code used to perform the analysis is provided as part of the code base, including the FIJI macro and the MATLAB scripts.

11.1   Extracting Trajectories from Raw Video Data

The raw video data is saved in .mp4 format by the Logitech software. We use ffmpeg to convert these files to .avi files for use with FIJI. Since .avi files are significantly larger in file size, we also downsample the videos to 5 frames per second (fps) while performing the file conversion. This reduced frame rate ensures a reasonable file size (approximately 400MB for videos of duration 1 minute) while preserving sufficient information for analysis. Note that our analysis is primarily concerned with extracting the net velocity and heading of the milliswimmers' trajectories, so reducing the frame rate will not have a substantial impact on our ability to accurately measure the total displacement of the milliswimmers.

Once all of the video files for a given experiment have been converted to .avi format and downsampled, we import them to FIJI. Our FIJI macro performs the following operations on each .avi file:

1. Open the file.

2. Prompt the user to crop the video to a region of interest. This is the only part of the process that requires manual user input. It requires the user to select a rectangular region that encloses the complete trajectory of the milliswimmer while minimizing the inclusion of any other features, including grid markings, the ruler, etc. This step is not automated as the milliswimmer's trajectory can vary, and there is minimal bias introduced in this step because the user must simply ensure that the full trajectory is included.

3. Once the user selects a region of interest, it is cropped.

4. The cropped video is reduced to an 8-bit range of pixel values.

5. The video is thresholded using the "Intermodes" algorithm.

6. The thresholded video is converted to a binary mask where the white pixels are part of the milliswimmer and the black pixels are the background.

7. The shapes formed by the white pixels are typically "Dilated" 4 times (in some cases we found that dilating for 1-2 additional times was necessary to correctly capture the entire swimmer and find the correct centroid). The dilation process adds pixels to the edges of the objects in the binary image, as described in the FIJI documentation. We perform this step in the case where there are gaps between white regions that comprise the milliswimmer, which can often form when some regions of the milliswimmer (such as the magnet) have less contrast than others. We know that the milliswimmer should be one contiguous object and we found that dilating 4 times generally expands the regions enough to form one object. Dilating the objects generally increases their size isometrically.

8. We set the measurements to include the area, the centroid and the center of mass of the particles found in the image.

9. The "Analyze Particles" feature is used to identify any objects within a size range of 1000 - 5500 pixels and to record their measurements as described in the previous step.

10. The results of the "Analyze Particles" function are saved to a .csv file for analysis in MATLAB.

11.2 Determining the Scale from Raw Video Data

Note that the data exported from the FIJI macro is reported in units of pixels and so we will need to convert the units to meters. To do this, we use FIJI to extract 5 measurements of a known distance in meters from 3 videos in the experiment set. Each video includes a view of a ruler in the frame, and we use FIJI to manually draw a line of length 1cm along the ruler in the videos. We draw 5 such lines and then use the Measurement tool in FIJI to record the distance in pixels. We can save this data to a .csv file. We repeat this process over 3 different videos selected at the beginning, middle and end of the experiment run to control for any variations in the scale over time. Our MATLAB script then imports the .csv files and uses the measurements to calculate an average conversion rate that we use to convert all measurements in pixels to meters.

11.3 Analyzing the Data in MATLAB

Once we have obtained our trajectory and scale data from FIJI, we can begin to analyze it in MATLAB. We use MATLAB to calculate the net velocity using the equation presented in the main text. We will exclude the first and last 3 seconds of data because there was a delay between the start (and end) of the video recording and the start (and end) of the magnetic field, as well as transient behaviors that do not affect the steady state velocity of the swimmers. We calculate the net velocity for each sample trajectory and then compute the mean and standard deviation over the 5 samples for each test. We plot the mean of these metrics with standard deviations shown as error bars.

12 Vibrating Sample Magnetometer Data Analysis

We wanted to measure the remanence of each magnet that we used to assemble a milliswimmer so that we could compare the remanences to the observed velocities for individual swimmers. To do, this we characterized the remanence of each milliswimmer using a vibrating sample magnetometer (Lakeshore).

Each swimmer was fixed onto a plastic sequin (cut in half) using sugar dissolved in deionized water as an "adhesive." The plastic sequin with the swimmer mounted upon it was then attached to the sample probe using double-sided tape. The sample probe surface was cleaned with ethanol after each sample. We measured the magnetic moment of 3 plastic sequins cut in half (and 2 fully circular plastic sequins, used to hold the longer large aspect ratio swimmers) to verify that the plastic sequins and double-sided tape did not make a substantial contribution to the measured remanence of the sample.

Before collecting measurements, the vibrating sample magnetometer (VSM) was calibrated and the external field was set to 0G. Note that the actual environment we used to test the swimming performance of the swimmers was nonzero, with an approximate magnitude of 3G for the $\beta = 1$ tests, and slightly larger magnitudes for the $\beta = 2$ and 3 tests (see the section on magnetometer data analysis for more information). However, the magnetic moment of a ferromagnet will increase monotonically from the magnet's remanence (i.e. the magnetic moment measured in the absence of an external field), so we can expect that magnets with larger remanence values will exhibit larger magnetic moments in non-zero fields as compared to magnets with smaller remanence values.

Once the VSM was calibrated, we mounted the sample (as described above) on the end of the sample probe and inserted it into the VSM. We then found the saddle point for the sample in question (this refers to the point where the measured field is a maximum in the y and z directions, and a minimum in the x direction) and then recorded the measurements of the magnetic moment for a period of 5 minutes, with a sampling rate of 0.1Hz, yielding a total of 30 measurements per sample.

References

[1] Nanoscribe. Nanoscribe photoresins specifically designed for Two-Photon Polymerization.

[2] J. Gray and G. J. Hancock. The Propulsion of Sea-Urchin Spermatozoa. *Journal of Experimental Biology*, 32(4), 1955.

[3] R. G. Cox. The motion of long slender bodies in a viscous fluid Part 1. General theory. *Journal of Fluid Mechanics*, 44(4):791–810, 12 1970.

[4] Emiliya Gutman and Yizhar Or. Simple model of a planar undulating magnetic microswimmer. *Physical Review E - Statistical, Nonlinear, and Soft Matter Physics*, 90(1):013012, 7 2014.

[5] Russell K. Hobbie and Bradley J. Roth. *Intermediate physics for medicine and biology, fifth edition*. Springer International Publishing, 1 2015.

[6] John Happel and Howard Brenner. Low Reynolds number hydrodynamics. 1, 1981.

[7] David J Detroye and Ronald J Chase. The Calculation and Measurement of Helmholtz Coil Fields. Technical report, 1994.

[8] Edward M. Purcell and David J. Morin. *Electricity and Magnetism*. Cambridge University Press, 3 edition, 2013.

[9] Thomas Kilgore Sherwood. *Mass transfer* . McGraw-Hill chemical engineering series. McGraw-Hill, New York, 1975.

[10] Johannes Schindelin, Ignacio Arganda-Carreras, Erwin Frise, Verena Kaynig, Mark Longair, Tobias Pietzsch, Stephan Preibisch, Curtis Rueden, Stephan Saalfeld, Benjamin Schmid, Jean Yves Tinevez, Daniel James White, Volker Hartenstein, Kevin Eliceiri, Pavel Tomancak, and Albert Cardona. Fiji: an open-source platform for biological-image analysis. *Nature Methods 2012 9:7*, 9(7):676–682, 6 2012.

[11] Chenyu Jiang, Panlong Gao, Xinsheng Yang, Dezheng Ji, Jialun Sun, and Zhenghao Yang. Helmholtz Coils Based WPT Coupling Analysis of Temporal Interference Electrical Stimulation System. *Applied Sciences 2022, Vol. 12, Page 9832*, 12(19):9832, 9 2022.